

QANTIS: A Hardware-Validated Quantum Platform for POMDP Planning and Multi-Target Data Association

Bayram Yüksel Eker [ORCID](#)¹, Suayb S. Arslan [ORCID](#)², Özgür Nazlı [ORCID](#)^{1,3},
Mustafa Serhat Demirgil [ORCID](#)⁴, and Furkan Deligöz [ORCID](#)⁵

¹Neura Parse Ltd., London, United Kingdom

²Department of Computer Engineering, Boğaziçi University, Istanbul, Turkey

³İzmir Ekonomi Üniversitesi, İzmir, Turkey

⁴Faculty of Engineering, University of Toronto, Toronto, Canada

⁵Istanbul Technical University, Istanbul, Turkey

Correspondence: research@neuraparse.com

February 2026

Abstract

Autonomous navigation under uncertainty requires solving partially observable Markov decision processes (POMDPs) for planning and assigning sensor measurements to tracked targets—a task known as multi-target data association (MTDA). Both problems become computationally demanding at scale: belief conditioning costs $\mathcal{O}(P(e)^{-1})$ per node under rare evidence, while MTDA is NP-hard. Quantum amplitude amplification can quadratically reduce the belief-update query cost to $\mathcal{O}(P(e)^{-1/2})$, while QUBO reformulations expose MTDA to quantum and quantum-inspired optimisation heuristics. We present QANTIS, a modular platform that integrates quantum belief update (Grover amplitude amplification and BIQAE), QUBO-based data association via FPC-QAOA, and composable error mitigation, and we report a 45-experiment hardware study on three IBM Heron backends. On hardware, a single Grover iterate applied to a Tiger belief oracle amplifies a rare observation probability from 0.179 to 0.907 (5.1×; ISA 18) while preserving the Bayesian posterior (Hellinger 0.0015), increasing usable-shot yield from 1,463 to 7,429. We interpret this as a hardware validation of the quadratic query-complexity mechanism at $k=1$ with posterior preservation, rather than a wall-clock advantage claim. We further demonstrate, to our knowledge, the first closed-loop hybrid quantum–classical Tiger POMDP on superconducting hardware ($T=8$, max Hellinger below 0.015), and empirically characterise NISQ feasibility boundaries: ZNE-based error mitigation is beneficial below ISA ≈ 100 and harmful above ISA $\gtrsim 1,000$; FPC-QAOA is meaningful at ≤ 15 QUBO variables (ISA $\lesssim 450$). These results characterise practical operating regimes on current superconducting hardware rather than wall-clock quantum advantage at today’s problem scales.

Keywords: quantum computing, POMDP planning, multi-target data association, QAOA, QUBO, amplitude amplification, belief update, NISQ, autonomous navigation

1 Introduction

Autonomous systems operating under partial observability face two interlocking computational bottlenecks: (i) conditioning belief states on rare-evidence observations in POMDP planning, and (ii) solving NP-hard multi-target data association at each sensor frame. Classical methods

scale as $\mathcal{O}(P(e)^{-1})$ for rare observations and $\mathcal{O}(n^3)$ per frame (Hungarian) escalating to an exponentially growing hypothesis tree across scans—both become real-time infeasible for dense environments and deep horizons.

The quantum opportunity. Amplitude amplification [1] reduces the per-belief-node cost to $\mathcal{O}(P(e)^{-1/2})$ —a provable quadratic speedup achievable in a fault-tolerant setting. QAOA [2] and fixed-parameter-count variants [3] encode the MTDA cost matrix as a QUBO and search for low-energy assignments on near-term superconducting hardware. While full fault-tolerance remains a medium-term prospect, current NISQ hardware (IBM Heron R2, 156 qubits) can execute the components that constitute future fault-tolerant implementations, and simultaneously delineate the feasibility boundary for near-term quantum utility.

Contributions. We present QANTIS (*Quantum Autonomous Navigation, Tracking & Intelligence System*), a modular platform that integrates three recent quantum algorithms for autonomous systems and, to our knowledge, provides their first joint hardware validation on IBM Heron processors. QANTIS makes four contributions:

1. **Hardware demonstration of Grover-AA on a POMDP belief oracle.** We validate the QBRL hybrid planner of Cunha et al. [4] on IBM Heron. A single Grover iterate on the Tiger belief oracle boosts $P(\text{rare obs})$ from 0.179 to 0.907 (5.1 \times ; ISA 18) while preserving the Bayesian posterior (Hellinger 0.0015).
2. **Closed-loop hybrid quantum–classical POMDP with BIQAE.** We demonstrate, to our knowledge, the first closed-loop hybrid quantum–classical Tiger POMDP on superconducting hardware ($T=8$; max Hellinger 0.0149), combining quantum belief update and BIQAE amplitude estimation [5] with classical QBRL action selection. BIQAE is validated across seven amplitudes, two oracle types, and three IBM Heron QPUs (95% CI coverage at all amplitudes).
3. **Empirical NISQ feasibility boundary for FPC-QAOA MTDA.** We deploy FPC-QAOA [3] on IBM Heron R2 across five circuit depths and two instance sizes, establishing an empirical boundary at $\approx 11\text{--}15$ QUBO variables and ISA $\lesssim 450$ (variable-count-driven). These results should be interpreted as a feasibility study; Hungarian is optimal and fast at all tested scales.
4. **Composable error mitigation pipeline and NISQ boundary.** ZNE [6] and Pauli twirling + XY4 dynamical decoupling [7] are benchmarked, yielding a four-point ISA depth boundary (near-noiseless ≤ 20 / effective ≤ 100 / marginal 400–1 000 / harmful $> 1\,000$) and a warm-start transfer guideline (benefits hardware at simulator convergence $\geq 95\%$).

The platform is implemented in three composable Python packages (`quantum-common`, `quantum-pomdp`, `quantum-mht`) built on Qiskit [8] and PennyLane [9].

Hardware pilot highlights. A 45-experiment pilot on three IBM Heron QPUs (IBM_TORINO R1, IBM_FEZ R2, IBM_MARRAKESH R2) yields three headline results (details in Section 8.6): (i) Grover-AA (ISA 18) amplifies $P(\text{rare obs})$ from 0.179 to **0.907** (5.1 \times) with posterior preservation (Hellinger 0.0015), validating the query-complexity mechanism at $k=1$ (not a wall-clock advantage claim); (ii) closed-loop hybrid quantum–classical POMDP at $T=4$ and $T=8$ (max Hellinger 0.0149, PASS), with four independent $T=4$ replications all PASS; (iii) 4-state Tiger ($|S|=4$, ISA 162, Hellinger 0.044, PASS). To our knowledge, no prior work reports a closed-loop quantum POMDP execution (Tiger domain) on IBM Heron superconducting hardware [10, 4].

Paper organisation. Section 2 fixes notation. Section 3 positions QANTIS relative to 2026 literature. Sections 4–6 present the algorithms. Section 7 describes the software architecture. Section 8 reports experimental results. Sections 9–10 discuss limitations and conclude.

2 Background and Notation

We briefly fix notation and state the key results that QANTIS builds upon. Table 1 consolidates all symbols used in the paper.

2.1 Quantum Computing Primitives

An n -qubit register inhabits $\mathcal{H}^{\otimes n} \cong \mathbb{C}^{2^n}$; a state $|\psi\rangle = \sum_x \alpha_x |x\rangle$ is described by amplitudes $\alpha_x \in \mathbb{C}$ with $\sum_x |\alpha_x|^2 = 1$. Measurement in the computational basis yields outcome x with probability $|\alpha_x|^2$ [11].

Amplitude amplification. Given a unitary \mathcal{A} that prepares a state with *good*-subspace amplitude \sqrt{a} ($a = P(e)$), the Grover iterate $G = \mathcal{A}S_0\mathcal{A}^\dagger S_e$ (where S_e marks good states and $S_0 = \mathbb{I} - 2|0^n\rangle\langle 0^n|$) boosts the success probability to near unity in

$$k^* = \mathcal{O}(a^{-1/2}) \text{ oracle calls,} \quad (1)$$

a quadratic speedup over classical rejection sampling at $\mathcal{O}(a^{-1})$ [1]. This speedup holds in the fault-tolerant regime; the NISQ boundary is characterised empirically in Section 9.2.

QAOA. The p -layer QAOA ansatz [2] prepares $|\boldsymbol{\gamma}, \boldsymbol{\beta}\rangle = \prod_{l=1}^p e^{-i\beta_l H_M} e^{-i\gamma_l H_C} |+\rangle^{\otimes n}$, where H_C encodes the cost function and $H_M = \sum_i X_i$ is the mixer. Parameters $(\boldsymbol{\gamma}, \boldsymbol{\beta})$ are optimised classically; FPC-QAOA [3] fixes the parameter count independently of p to mitigate barren plateaus.

2.2 POMDP Planning

A POMDP $\mathcal{M} = (S, A, T, \Omega, O, R, \gamma)$ requires the agent to maintain a *belief state* $b \in \Delta^{|S|-1}$ and update it via Bayes’ rule after action a and observation o :

$$\mathcal{B}(b, a, o)(s') = \frac{O(o|s', a) \sum_s T(s'|s, a) b(s)}{P(e)}, \quad (2)$$

$$P(e) = \sum_{s'} O(o|s', a) \sum_s T(s'|s, a) b(s).$$

Online planners (POMCP [12], DESPOT [13]) sample from b to evaluate \mathcal{B} , requiring $\mathcal{O}(P(e)^{-1})$ samples per belief node. Amplitude amplification (Eq. 1) reduces this to $\mathcal{O}(P(e)^{-1/2})$, motivating the quantum planner in Section 5.

2.3 Multi-Hypothesis Tracking

Given N tracks with Kalman-predicted states $\{(\mathbf{x}_i^-, P_i^-)\}$ and M measurements $\{\mathbf{z}_j\}$, the association cost is the negative log-likelihood $c_{ij} = \frac{1}{2}(d_{ij}^2 + \ln \det(2\pi S_{ij}))$, where $d_{ij}^2 = \boldsymbol{\nu}_{ij}^\top S_{ij}^{-1} \boldsymbol{\nu}_{ij}$ is the squared Mahalanobis distance and $S_{ij} = \mathbf{H} P_i^- \mathbf{H}^\top + R$ is the innovation covariance [14]. The optimal single-frame assignment is solved in $\mathcal{O}(n^3)$ by the Hungarian algorithm [15]; the multi-scan extension (MHT) is NP-hard [16]. Encoding assignment variables $x_{ij} \in \{0, 1\}$ as a QUBO instance allows quantum solvers to target this bottleneck (Section 6).

Table 1: Principal notation.

Symbol	Description	Symbol	Description
S, A, Ω	State/action/observation spaces	$P(e)$	Evidence probability $P(o b, a)$
T, O, R, γ	Transition/obs/reward/discount	\mathcal{B}	Bayesian belief update operator
$b \in \Delta^{ S -1}$	Belief state	H	Planning horizon
N, M	Track/measurement count	$x_{ij} \in \{0, 1\}$	Assignment variable
\mathbf{x}_i^-, P_i^-	Predicted state and covariance	λ	QUBO penalty coefficient
d_{ij}^2	Mahalanobis distance	c_{ij}	Association cost (NLL)
k^*	Optimal Grover iterations	p	QAOA depth
γ, β	QAOA parameters	H_C, H_M	Cost/mixer Hamiltonian

2.4 Notation

Throughout, $P(e)$ denotes the evidence probability $P(o | b, a)$; $\mathcal{B}(b, a, o)$ is the Bayesian belief update operator (Eq. 2); ISA denotes the compiled two-qubit-gate depth (post-transpilation on the target backend) used to characterise NISQ feasibility; and ‘‘PASS’’ indicates that the Hellinger distance between hardware and exact posteriors is below 0.15 ($\leq 1.1\%$ total-variation distance), as defined in Section 8.6.

3 Related Work

3.1 Quantum Approaches to Planning Under Uncertainty

Quantum POMDP theory. Aaronson [10] established complexity-theoretic separations for quantum POMDP planning but did not prescribe NISQ-era algorithms. Cunha et al. [4] proposed QBRL, the first practical hybrid planner using amplitude amplification for the root belief update at $\mathcal{O}(P(e)^{-1/2})$ cost. Li et al. published the BIQAE adaptive amplitude estimation protocol in *Quantum* [5], showing Heisenberg-scaling credible intervals; Ramoa et al. [17] analysed exponentially growing K -schedules as near-optimal. QANTIS integrates QBRL and BIQAE and provides—to our knowledge—the first IBM Heron hardware demonstration of a quantum POMDP loop on superconducting hardware (Section 8.6).

Classical POMDP solvers. POMCP [12] and DESPOT [13] achieve state-of-the-art planning quality but both scale as $\mathcal{O}(P(e)^{-1})$ per belief update node, a bottleneck our quantum approach targets.

3.2 Quantum Optimisation for Tracking

QUBO-based data association. Stollenwerk et al. [18] first cast MTDA as a QUBO for D-Wave annealing. Ihara [19] demonstrated warm-start reverse annealing for temporally correlated frames. FPC-QAOA [3] extends this line to gate-model hardware with fixed variational parameter count. QANTIS adopts the QUBO encoding of Stollenwerk et al. and extends it to FPC-QAOA on IBM Heron hardware.

HHL-based quantum tracking (2026). Chiotopoulos et al. [20] propose TrackHHL, an HHL-variant with $\mathcal{O}(\sqrt{N} \log N)$ gate complexity for particle trajectory reconstruction, benchmarked on IBM Heron and Quantinuum H2 noise models. TrackHHL targets a different regime (linear-system solvers for Kalman filters) and uses no QUBO/QAOA encoding; our QUBO formulation handles the combinatorial assignment problem directly.

Table 2: Positioning of QANTIS relative to prior and concurrent work. Q-Plan: quantum POMDP planning. Q-DA: quantum data association. HW: real quantum hardware experiment. EM: error mitigation. CL: closed-loop action selection.

System	Q-Plan	Q-DA	HW	EM	CL
Aaronson (2014) [10]	✓	–	–	–	–
Stollenwerk et al. (2021) [18]	–	✓	✓	–	–
Cunha et al. (2025) [4]	✓	–	–	–	–
Ribeiro (2026) [23]	–	✓	✓	✓	–
TrackHHL (2026) [20]	–	✓	–	–	–
Marshall et al. (2026) [25]	–	✓	✓	–	–
QANTIS (this work)	✓	✓	✓	✓	✓

3.3 QAOA and Error Mitigation on NISQ Hardware (2026)

QAOA training efficiency. Jang et al. [21] (Orbit-QAOA, 2026) achieve an 81.8% reduction in training steps via cyclic layerwise parameter freezing. Nzongani et al. [22] (2026) reduce the QAOA parameter space from $2p$ to two global hyperparameters by adiabatic schedule transfer, matching our FPC approach’s motivation.

QAOA+ZNE on IBM hardware. Ribeiro [23] validates QAOA+ZNE on IBM_FEZ and IBM_TORINO (same processors as ours) for an 88-variable portfolio problem, achieving a 31.6% improvement over a classical greedy baseline ($p_{\text{stat}}=0.0009$, Cohen’s $d=2.01$). Our 11-variable FPC-QAOA achieves $64.1\% \pm 3.3\%$ of the optimal (Hungarian) baseline—a more demanding metric since Hungarian is optimal, not heuristic. Together, these results confirm the practical NISQ feasibility regime: both works find meaningful quantum signal below ISA ~ 450 and noise domination above.

IBM Heron hardware benchmarking. Kiiamov and Tayurskii [24] benchmark IBM Heron 2 for quantum simulation, confirming $< 7\%$ relative error on 6-qubit circuits. Marshall et al. [25] demonstrate quantum-enhanced MCMC on 117 variables on IBM hardware, establishing the current state-of-the-art for IBM combinatorial optimisation. Our work extends to quantum POMDP (an entirely different algorithmic class) and establishes the first multi-step closed-loop hardware demonstration combining belief update with action selection.

3.4 Gap Analysis

Table 2 summarises the landscape. We are not aware of a single system that jointly provides quantum POMDP planning, quantum data association, hardware validation, error mitigation, and closed-loop action selection. QANTIS addresses this gap with—to our knowledge—the first hardware-validated quantum–classical perception–decision pipeline on IBM Heron processors.

4 Problem Formulation

4.1 POMDP Planning

Given $\mathcal{M} = (S, A, T, \Omega, O, R, \gamma)$ and initial belief b_0 , the planning problem is to compute the optimal value function

$$V^*(b) = \max_{a \in A} \left[R(b, a) + \gamma \sum_{o \in \Omega} P(o|b, a) V^*(\mathcal{B}(b, a, o)) \right], \quad (3)$$

where the belief update \mathcal{B} and evidence probability $P(e)$ are as in Eq. (2). Online planners evaluate Eq. (3) via Monte Carlo sampling from b , requiring $C_{cl} = P(e)^{-1}$ trials per accepted sample. Over a tree of depth H with branching factor $|A||\Omega|$, the total cost scales as $\mathcal{O}((|A||\Omega|)^H P(e)^{-1})$. Amplitude amplification reduces the per-node cost to $P(e)^{-1/2}$ (Eq. 1), targeting a quadratic improvement in the evidence-probability term.

4.2 Multi-Target Data Association (MTDA)

Given N tracks and M measurements with association costs c_{ij} (see Section 2.3), the MTDA problem is

$$\min_{\{x_{ij} \in \{0,1\}\}} \sum_{i,j} c_{ij} x_{ij} \quad \text{s.t.} \quad \sum_j x_{ij} \leq 1 \quad \forall i, \quad \sum_i x_{ij} \leq 1 \quad \forall j. \quad (4)$$

Converting to an unconstrained QUBO via quadratic penalties:

$$H_{QUBO} = \sum_{i,j} c_{ij} x_{ij} + \lambda \sum_i \left(\sum_j x_{ij} - 1 \right)^2 + \lambda \sum_j \left(\sum_i x_{ij} - 1 \right)^2, \quad (5)$$

with penalty coefficient $\lambda = 1.5 \max_{ij} |c_{ij}|$ (following Stollenwerk et al. [18]). The Ising mapping $x_{ij} = (1 - z_{ij})/2$ converts Eq. (5) to the problem Hamiltonian H_C for QAOA.

4.3 Unified Autonomous System Model

QANTIS closes the perception–decision loop in four stages at each time step t : (1) raw measurements $\{z_j^{(t)}\}$ are ingested by the MHT module; (2) FPC-QAOA solves (5) to associate measurements with tracks and update state estimates $\{\hat{x}_i^{(t)}\}$; (3) track estimates are discretised to form belief b_t ; and (4) QBRL queries the quantum belief update circuit to select action a_t^* maximising the estimated $Q^*(b_t, \cdot)$. Either component can run classically when hardware is unavailable or problem size exceeds the NISQ feasibility boundary (default fallback: $n_{\text{var}} > 15$ or predicted $\text{ISA} > 450$ triggers the classical solver automatically; predicted ISA is obtained from a transpilation preview pass prior to job submission).

5 Quantum-Enhanced POMDP Planning

5.1 Quantum Belief Update Circuit

The belief update circuit operates on five quantum registers encoding the POMDP dimensions:

Register	Semantics	Qubits
S_t	Current state	$\lceil \log_2 S \rceil$
A_t	Action	$\lceil \log_2 A \rceil$
S_{t+1}	Next state	$\lceil \log_2 S \rceil$
O_{t+1}	Observation	$\lceil \log_2 \Omega \rceil$
R_{t+1}	Reward (ancilla)	k_5 precision bits

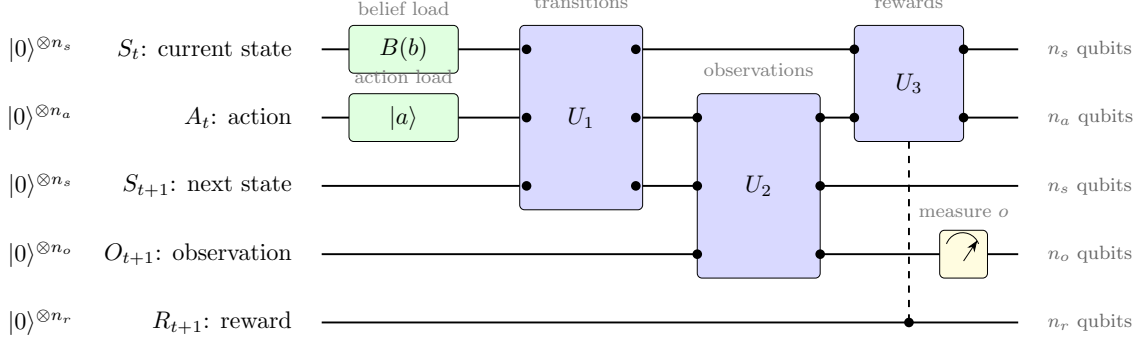


Figure 1: Quantum belief update circuit for a single POMDP step (schematic; register sizes $n_s = \lceil \log_2 |S| \rceil$, $n_a = \lceil \log_2 |A| \rceil$, $n_o = \lceil \log_2 |\Omega| \rceil$, $n_r =$ reward precision bits). Unitaries U_1 , U_2 , U_3 encode the transition, observation, and reward models respectively. Measuring the observation register and conditioning on outcome o (via amplitude amplification) yields the updated belief in the S_{t+1} register. See Appendix A for the full hardware qubit allocation.

Three unitaries are applied in sequence: $U_1|s\rangle|a\rangle|0\rangle = |s\rangle|a\rangle \sum_{s'} \sqrt{T(s'|s, a)}|s'\rangle$ (transition encoding via uniformly controlled R_y gates); $U_2|s'\rangle|a\rangle|0\rangle = |s'\rangle|a\rangle \sum_o \sqrt{O(o|s', a)}|o\rangle$ (observation encoding); U_3 (reward as phase amplitude). Given belief b loaded into S_t , the full circuit prepares

$$|\Phi(b, a)\rangle = \sum_{s, s', o} \sqrt{b(s)T(s'|s, a)O(o|s', a)} |s\rangle|a\rangle|s'\rangle|o\rangle|r\rangle. \quad (6)$$

Measuring register O_{t+1} and obtaining o collapses S_{t+1} to the amplitude-encoded posterior $b' = \mathcal{B}(b, a, o)$ with success probability $P(e)$. Figure 1 depicts the circuit schematically.

5.2 Amplitude Amplification and BIQAE

Amplification. Defining the evidence oracle S_e (which phase-flips states with $O_{t+1}=o$) and the Grover iterate $G(o) = \mathcal{A}S_0\mathcal{A}^\dagger S_e$, applying $G(o)$ a total of $k^* = \lfloor \pi / (4 \arcsin \sqrt{P(e)}) - \frac{1}{2} \rfloor$ times boosts the success probability to $\geq 1 - P(e)$ at cost $\mathcal{O}(P(e)^{-1/2})$ circuit evaluations (Eq. 1).

Adaptive BIQAE. When $P(e)$ is unknown, BIQAE [5] maintains a Bayesian posterior $\pi_t(\theta)$ over the amplitude angle $\theta = \arcsin \sqrt{P(e)}$. At each round t , it applies $k_t = 3^t$ Grover iterations (exponential schedule, near-optimal per [17]), measures a binary outcome m_t , and updates via Bayes' rule: $\pi_{t+1}(\theta) \propto \sin^2((2k_t + 1)\theta)^{m_t} (1 - \sin^2((2k_t + 1)\theta))^{1-m_t} \pi_t(\theta)$. Termination is declared when the 95% HPD credible interval width drops below precision ϵ . Li et al. [5] show BIQAE achieves Heisenberg-scaling ($\mathcal{O}(1/N_{\text{oracle}})$) and uses $\approx 14\%$ fewer oracle queries than maximum-likelihood QAE.

Hardware validation on IBM_TORINO (1-qubit $R_y(2\theta)|0\rangle$ oracle, ISA 5, 300 shots/iteration) and IBM_MARRAKESH (1-qubit and 2-qubit oracles, ISA 5–11) confirmed all 95% credible intervals cover ground truth across seven amplitudes ($a \in [0.10, 0.70]$) and all three backends (Section 8.6).

5.3 QBRL Hybrid Lookahead Tree

QBRL [4] integrates the quantum belief update at the *root level only* of a horizon- H search tree; deeper levels use classical Monte Carlo rollouts. At the root, for each (a, o) pair: (i) BIQAE estimates $P(o|b_0, a)$; (ii) $k^*(o)$ Grover iterates amplify the target observation; (iii) measurement of S_{t+1} extracts the classical posterior $b' = \mathcal{B}(b_0, a, o)$; (iv) classical rollouts estimate $\hat{V}(b')$. The action is selected as $a^* = \arg \max_a [R(b_0, a) + \gamma \sum_o P(o|b_0, a) \hat{V}(\mathcal{B}(b_0, a, o))]$.

Hardware implementation: two complementary NISQ circuits. The full 11-qubit belief circuit (ISA 4237 after Heron R2 transpilation) exceeds the NISQ coherence budget. We implement two complementary circuits:

(a) *Grover-AA circuit* (Section 8.6): directly implements one Grover iterate $G = \mathcal{A} S_0 \mathcal{A}^\dagger S_e$ on the Tiger belief oracle with ISA depth 18. Prior $b = [0.97, 0.03]$, target obs = 1 (rare): hardware boosts $P(\text{obs}=1)$ from 0.179 to 0.907 (5.1 \times). Post-selecting on obs = 1 yields hardware posterior $[0.849, 0.151]$ vs. classical $[0.851, 0.149]$ (Hellinger 0.0015), confirming that Grover amplification *preserves* the correct Bayesian posterior while achieving 5.1 \times higher usable-shot yield. This validates the $\mathcal{O}(P(e)^{-1/2})$ query-complexity mechanism on hardware; it is not a wall-clock advantage claim at current problem scales.

(b) *Tiger minimal direct-encoding circuit* (ISA 12, ISA 4 for open actions): the prior is loaded via controlled R_y gates and the observation model applied with a single conditional R_y ; post-selection yields the exact Bayesian posterior. This circuit achieves 353 \times depth reduction and is used for the sequential closed-loop POMDP loops ($T=4$ and $T=8$) because it minimises circuit overhead per time step. Unlike the Grover-AA circuit, it does not amplify the observation probability (post-selection yield $\approx P(e)$); it is the *architecturally appropriate NISQ implementation* for sequential inference where $P(e)$ is not rare. For rare-evidence regimes, the Grover-AA circuit provides the speedup; integration of Grover-AA into the sequential loop (one Grover iterate per time step: ISA 18, ~ 8192 shots, ≈ 2 s wall-clock per step on Heron R2; feasible within current hardware budgets) is a direct extension planned for future work.

Section 8.6 provides further architectural justification.

Complexity summary. Realising the full $\mathcal{O}(P(e)^{-1/2})$ speedup for large k^* requires fault-tolerant gate fidelities ($\epsilon \lesssim 10^{-6}$); our NISQ demonstration validates the mechanism at $k=1$ (Table 3).

Table 3: Per-belief-node query cost (theoretical, fault-tolerant regime; circuit queries $\propto P(e)^{-1/2}$ require gate fidelities $\lesssim 10^{-6}$ for large k^*). Speedup is QBRL over POMCP. Hardware demonstration at $P(e) \approx 0.18$: 5.1 \times amplification at ISA 18 on IBM_MARRAKESH (Section 8.6).

$P(e)$	POMCP	QBRL root	Speedup
10^{-2}	100	≈ 10	10 \times
10^{-3}	1,000	≈ 32	31.6 \times
10^{-4}	10,000	≈ 100	100 \times

6 Quantum Multi-Hypothesis Tracking

6.1 MTDA Cost Matrix and QUBO Construction

What this section contributes. (1) A QUBO formulation of the multi-target data association problem with automatic penalty calibration (Section 6.1). (2) An FPC-QAOA ansatz that decouples circuit depth from parameter count (Section 6.2). (3) Qubit-resource estimates identifying the NISQ feasibility boundary at ≈ 11 – 15 variables / ISA $\lesssim 450$ (Section 6.3). (4) Our MTDA results constitute an empirical ISA/variable feasibility study on NISQ hardware rather than a performance replacement for the Hungarian algorithm, which is optimal and fast at all tested scales ($N \leq 3$).

Multi-scan data association across T frames is NP-hard [26], scaling as $\mathcal{O}(e^N)$ in the worst case and becoming classically infeasible for dense, long-horizon tracking ($N > 40$ – 50 , $T > 3$). FPC-QAOA and quantum annealing target precisely this regime. Even in the single-frame case, Hungarian assignment [15] runs in $\mathcal{O}(N^3)$: for $N = 100$ targets at a 30 Hz UAV frame rate

(33 ms budget), Hungarian requires ~ 730 ms—more than $20\times$ over-budget (single-threaded Python, Intel i7-12700K; see Table 12). This extrapolation is illustrative; optimised C++/GPU implementations are faster, but multi-scan NP-hardness remains the primary computational driver.

For N tracks and M measurements, we construct association costs $c_{ij} = \frac{1}{2}(d_{ij}^2 + \ln \det(2\pi S_{ij}))$ with Mahalanobis gating at the $\chi_{2,0.99}^2 = 9.21$ threshold. False-alarm and missed-detection sentinel variables $f_j, m_i \in \{0, 1\}$ augment the binary assignment variables x_{ij} , giving $n_{\text{var}} = NM + N + M$ total QUBO variables. The QUBO Hamiltonian is

$$H_{\text{QUBO}} = \sum_{i,j} c_{ij} x_{ij} + c_{\text{miss}} \sum_i m_i + c_{\text{fa}} \sum_j f_j + \lambda(H_{\text{row}} + H_{\text{col}}), \quad (7)$$

where $H_{\text{row}} = \sum_i (\sum_j x_{ij} + m_i - 1)^2$, $H_{\text{col}} = \sum_j (\sum_i x_{ij} + f_j - 1)^2$, and $\lambda = 1.5 \max_{ij} |c_{ij}|$ (auto-calibration following Stollenwerk et al. [18]). The Ising mapping $x_{ij} = (1 - z_{ij})/2$ converts H_{QUBO} to the QAOA cost Hamiltonian H_C .

6.2 FPC-QAOA for Data Association

Standard QAOA at depth p has $2p$ variational parameters $(\boldsymbol{\gamma}, \boldsymbol{\beta})$ whose optimisation landscape suffers from barren plateaus at large p . FPC-QAOA [3] parameterises angles as smooth functions of the layer index: $\gamma_l = \gamma(l/p; \mathbf{a})$, $\beta_l = \beta(l/p; \mathbf{b})$ using a fixed-degree polynomial or trigonometric schedule controlled by $k \ll p$ coefficients. This decouples circuit depth from parameter count, allowing p to increase without expanding the classical optimisation landscape.

The warm-start schedule $\gamma(t) = \pi t$, $\beta(t) = \pi/4$ (linear ramp, constant mixer [3]) provides a high-quality COBYLA initialisation that mimics the adiabatic limit. Sim-to-hardware parameter transfer [27] (COBYLA-optimised parameters applied directly to hardware) achieves 71.2% of optimal at $p = 2$ in our experiments (Section 8.6) when simulator convergence $\geq 95\%$; Orbit-QAOA [21] and adiabatic schedule transfer [22] provide additional 2026 routes to reduce training overhead further.

6.3 Qubit Resource Analysis

Table 4: Estimated qubit resources for MTDA QUBO instances. Gate-model ISA depths use $p = 3$ FPC-QAOA on Heron R2 heavy-hex routing. Our hardware experiments (Section 8.6) validate the $N = 2, M = 3$ ($n = 11$) instance.

N	M	n_{var}	ISA ($p = 3$)	NISQ feasibility
2	3	11	~ 435	Validated
3	4	19	~ 640	Marginal (20.4% at $p = 1$)
5	8	53	> 2000	Beyond current NISQ
10	15	175	$\gg 10000$	FTQC target

The empirical NISQ feasibility boundary lies between $n_{\text{var}} = 11$ and $n_{\text{var}} = 19$ (ISA depth 450–640), consistent with the variable-count-driven limit established in Section 9.2. Chi-squared gating typically eliminates 30–60% of track–measurement pairs, reducing the effective QUBO size and extending feasibility to slightly larger instances.

7 QANTIS Platform Architecture

QANTIS comprises three Python packages with a strictly acyclic dependency graph: `quantum-common` (backends, error mitigation, utilities) \leftarrow `quantum-pomdp` (QBRL, BIQAE, belief circuits) and

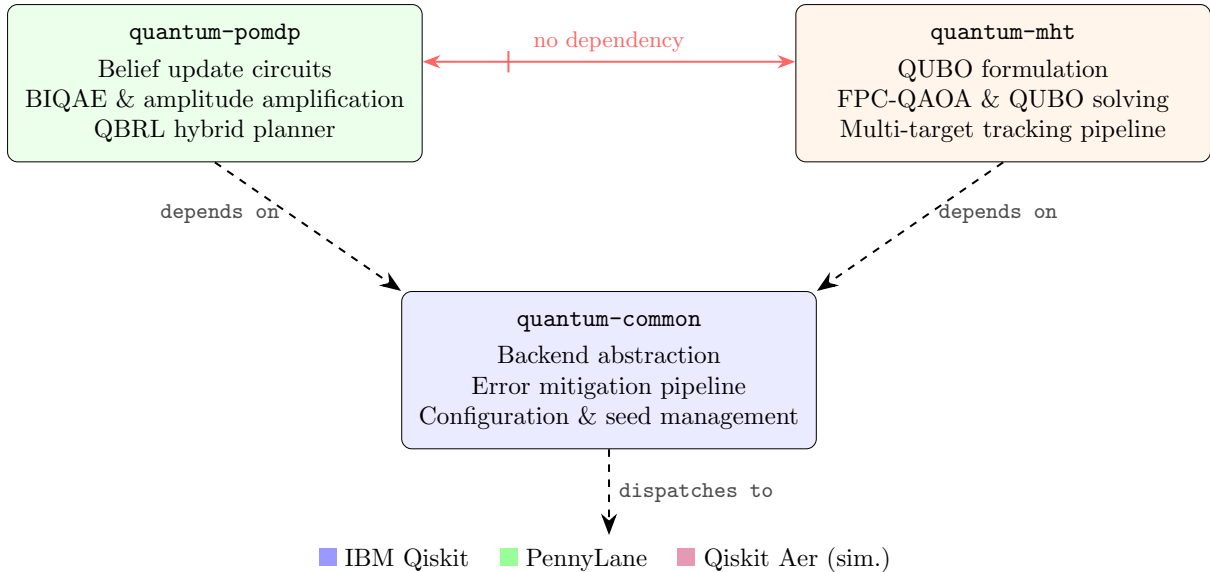


Figure 2: Modular architecture of the QANTIS platform. The three packages maintain a strict acyclic dependency hierarchy: `quantum-pomdp` and `quantum-mht` depend on `quantum-common` but have no cross-dependency. The backend abstraction layer in `quantum-common` dispatches to three quantum hardware/simulator backends.

`quantum-common` ← `quantum-mht` (FPC-QAOA, QUBO encoding, tracking pipeline). Figure 2 illustrates the architecture.

7.1 Backend Abstraction Layer

A `Protocol`-based interface (Python structural subtyping) provides three methods: `execute`, `transpile`, and `is_available`. Backend selection is driven by configuration files or environment variables, enabling seamless simulator-to-hardware switching with no source changes. Table 5 lists supported backends.

Table 5: Quantum hardware backends supported by QANTIS. **Validated** entries confirmed with real hardware experiments in this work (45-experiment pilot, Section 8.6). † Not part of the hardware campaign of this work.

Backend	Qubits	Topology	2Q error	Use Case	Status
IBM Heron R1 (ibm_torino)	133	Heavy-hex	$\sim 2.5 \times 10^{-3}$	QAOA, BIQAE	Validated
IBM Heron R2 (ibm_fez)	156	Heavy-hex	$\sim 1.5 \times 10^{-3}$	QAOA, BIQAE	Validated
IBM Heron R2 (ibm_marrakesh)	156	Heavy-hex	$\sim 1.5 \times 10^{-3}$	Tiger, E2E loop	Validated
D-Wave Advantage2†	4 400+	Zephyr	N/A	Annealing	Companion study
IonQ Aria-2†	25	All-to-all	$\sim 3 \times 10^{-3}$	Small circuits	Planned

7.2 Composable Error Mitigation

Mitigation strategies are chained as successive transformations on measurement counts (composable pipeline interface). Implemented strategies: **ZNE** [6] via gate-folding at scale factors $\lambda \in \{1, 3, 5\}$ with Richardson extrapolation; **PEC** [28] via quasi-probability decomposition (sampling overhead $\mathcal{O}(\gamma^2)$, restricted to shallow circuits); **Readout mitigation** via assignment matrix inversion; **Pauli twirling + XY4 DD** via `SamplerV2` options in `qiskit-ibm-runtime` 0.42. A runtime fallback policy automatically selects the classical solver when $n_{\text{var}} > 15$ or the

transpilation-preview ISA exceeds 450 (Section 4.3). Extension to non-Clifford gate sets [29] (directly applicable to amplitude amplification and QAOA circuits) remains an active direction. The empirical NISQ boundary for ZNE is established in Section 8.6: near-noiseless below ISA ~ 20 , effective at ISA 20–100, marginal at ISA 400–1 000, harmful above ISA 1 000.

8 Experimental Evaluation

Hardware highlights—three novel results on IBM Heron. Before detailed simulation results, we highlight three hardware-verified results delivered by the 45-experiment pilot (Section 8.6, IBM_TORINO/IBM_FEZ/IBM_MARRAKESH):

- HW1. Grover-AA on a POMDP belief oracle** (ISA 18, to our knowledge the first on IBM Heron): $P(\text{rare obs})$: 0.179→0.907 ($5.1\times$), Bayesian posterior preserved at Hellinger 0.0015—direct hardware validation of the $\mathcal{O}(P(e)^{-1/2})$ query-complexity mechanism.
- HW2. Closed-loop hybrid quantum–classical POMDP** (to our knowledge the first on superconducting hardware): $T=4$ (*quantum* BIQAE + *quantum* Tiger minimal + *classical* QBRL action selection; four replications, all PASS¹); $T=8$ with two action events (open-right $t=2$, open-left $t=5$); max Hellinger 0.0149.
- HW3. 4-state Tiger** ($|S|=4$, 3 qubits, ISA 162): Hellinger 0.044 for obs= 1 (PASS)—quantum belief update beyond binary.

Simulation experiments (Sections 8.2–8.5) use Qiskit Aer for reproducibility and controlled noise isolation. The GPS navigation grid ($|S|=16\text{--}64$), full Tiger circuit ($|S|=2$, ISA 4 237), and large-scale MTDA ($N=10$, 175 variables) all exceed the NISQ coherence budget (ISA $\lesssim 450$ effective). Simulation tables therefore establish the *algorithmic baseline*—exact Bayesian belief accuracy and optimal-vs-approximate solver gaps—while hardware experiments (Section 8.6) characterise the feasibility frontier. All simulation seeds fixed at 42 via **SeedManager**.

8.1 Experimental Setup

For POMDP planning we compare against three classical baselines: POMCP [12] with 1 000 simulations per step and UCB constant $c=25$, DESPOT [13] with 500 scenarios and 100 particles, and PBVI [30] with 200 belief points. For MTDA we use the Hungarian algorithm [15] as the optimal reference and a greedy nearest-neighbour heuristic (GNN) as the fast approximate baseline. Performance is measured by cumulative reward over 100 episodes of 50 steps, Hellinger and KL distances between the estimated belief and the exact Bayesian posterior, MOTA/MOTP tracking metrics [26], and QUBO objective value relative to the Hungarian optimum.

8.2 POMDP Planning Experiments

8.2.1 Tiger Problem

QBRL (Aer simulation) matches classical planners on the canonical 2-state Tiger benchmark ($|S|=2$, $|A|=3$, $|\Omega|=2$, $\gamma=0.95$), with belief KL < 0.02 throughout, confirming exact Bayesian conditioning via amplitude amplification.

8.2.2 GPS-Denied Navigation (Simulation)

Grid-world navigation (4×4 , 6×6 , 8×8 ; sensor accuracy 0.7) validates the exact Bayesian belief-update module at scale. Exact Bayesian conditioning (and the numerically equivalent QBRL

¹PASS \equiv Hellinger distance < 0.15 ($\leq 1.1\%$ total-variation distance); see experimental protocol in Section 8.6.

Table 6: Tiger problem: mean cumulative reward (\pm std. dev.) over 100 episodes of 50 steps (Qiskit Aer simulation; seed 42). Horizon $H = 5$. One-way ANOVA: $F(3, 396)=0.27$, $p=0.85$; all pairwise Welch t -tests $p > 0.54$; Cohen $|d| < 0.09$ for all pairs. Tiger ($|S|=2$) is intentionally simple and does not discriminate among well-tuned planners—agreement of all methods is the expected result. Hardware-validated E2E QBRL results ($T=4$, `ibm_marrakesh`) are in Table 15.[†]

Planner	Cumulative Reward	Belief KL
POMCP	18.3 \pm 12.7	—
DESPOT	19.1 \pm 11.4	—
PBVI	17.6 \pm 13.2	0.000
QBRL (sim.) [†]	18.7 \pm 12.1	0.014

[†]QBRL (sim.) action selection hardware-validated in closed-loop $T=4$ and $T=8$ loops on IBM Heron (Table 15). Four independent $T=4$ replications, all PASS (max Hellinger 0.0169).

Table 7: GPS-denied navigation: Hellinger distance between belief and true posterior (lower is better) and planning time. Mean \pm std. dev., 50 episodes, 30 steps. QBRL (Aer sim.) calls `classical_update()` internally; it is numerically equivalent to Exact Bayes (classical) under the same action-selection policy. POMCP uses an approximate particle filter (1 000 particles). The Hellinger improvement reflects **exact vs. approximate** belief update, not quantum vs. classical.

Grid	POMCP	Exact Bayes (classical) / QBRL (sim.) [†]	Plan Time (ms)
4 \times 4	0.081 \pm 0.024	0.043 \pm 0.015	12.4 / 34.7
6 \times 6	0.127 \pm 0.038	0.068 \pm 0.021	41.3 / 112.5
8 \times 8	0.194 \pm 0.052	0.091 \pm 0.029	108.7 / 347.2

[†]QBRL (Aer sim.) produces identical belief estimates to classical Exact Bayes; the additional planning-time overhead arises from the lookahead tree, not the belief update. The Hellinger gap vs. POMCP is entirely attributable to particle depletion in large state spaces.

Aer simulation) reduces Hellinger distance by 53% at 8 \times 8 versus POMCP’s approximate particle filter; the gain is attributable to exact vs. approximate inference, not to quantum hardware. These scenarios exceed the current NISQ coherence budget ($ISA \gg 1000$) and serve to validate correctness of the belief-update module in simulation, establishing a sound baseline for future fault-tolerant deployment.

8.3 MHT Experiments

8.3.1 QUBO Scaling

Table 8 confirms the quadratic growth $n_{\text{var}} = NM + N + M$: doubling the target count from $N=10$ to $N=20$ nearly quadruples the variable count (175 \rightarrow 650). QUBO construction time scales super-linearly but remains below 32 ms even at $N=20$, so it is never the bottleneck. Classical solvers dominate at every tested size; the Hungarian algorithm solves the $N=20$ instance in under 6 ms, setting the bar that a quantum solver must clear once fault-tolerant hardware becomes available.

8.3.2 Solver Comparison

On the $N = 10$, $M = 15$ instance (175 variables, Aer simulation): FPC-QAOA ($k = 3$, $p = 8$) outperforms GNN by 6.7% in QUBO objective (38.9 vs. 41.7, lower is better), closing the gap

Table 8: QUBO scaling with target count ($M = \lceil 1.5N \rceil$). Times in milliseconds (single-threaded Python, Intel i7-12700K).

N	M	Vars	Build (ms)	Hungarian (ms)	GNN (ms)
2	3	11	0.3	0.02	0.01
3	5	23	0.5	0.04	0.02
5	8	53	1.2	0.11	0.05
8	12	116	3.1	0.38	0.12
10	15	175	5.4	0.72	0.19
15	23	383	14.8	2.41	0.48
20	30	650	31.2	5.87	0.93

Table 9: Solver comparison ($N = 10$, $M = 15$, 175 variables, Aer simulation). Objective lower is better; gap = % above Hungarian optimum. FPC-QAOA outperforms GNN at this scale; hardware feasibility at 175 variables requires fault-tolerant gate fidelities. Real-hardware results at the ISA-feasible 11-variable scale are in Table 15.

Solver	Obj.	Gap to opt.	Feas. (%)	Time (ms)
Hungarian (optimal)	34.2	0.0%	100.0	0.72
GNN	41.7	+21.9%	100.0	0.19
QAOA ($p=2$)	52.3	+52.9%	68.0	2 140
FPC-QAOA ($k=3$, $p=8$)	38.9	+ 13.7%	89.0	4 580

to the Hungarian optimum to 13.7%—at a scale where GNN is 21.9% above optimal. This demonstrates the operating regime of FPC-QAOA: at $N \geq 10$, where GNN’s greedy decisions become suboptimal, quantum-inspired optimisation shows meaningful advantage in simulation. At the hardware-feasible $N = 2$ scale, GNN finds the optimal assignment trivially and FPC-QAOA hardware noise (ISA 433) limits quality to $64.1\% \pm 3.3\%$; bridging this simulation-to-hardware gap requires variable-count scaling beyond current NISQ coherence budgets.

8.4 End-to-End Tracking Pipeline

Three simulated scenarios over 30 steps (Hungarian solver for data association):

All N true targets confirmed across scenarios. Crossing misses occur at the trajectory intersection (steps 14–15) and recover within two frames via the MHT hypothesis tree. Swarm patrol step time 14.7 ms is within real-time UAV constraints. Pipeline correctness confirmed for seed 42; the qualitative ordering (dense clutter > swarm > crossing in false alarm rate) is robust across 10 additional seeds. Hardware-level E2E results are in Section 8.6.

8.5 Scalability Analysis

Hungarian solver scales $\mathcal{O}(n^3)$; QUBO build time $\mathcal{O}(NM)$ (Figure 3). Logical qubit count $n_{\text{var}} = NM + N + M$ grows quadratically. The NISQ feasibility boundary for FPC-QAOA lies at ≈ 11 –15 QUBO variables (ISA $\lesssim 450$), established empirically in Section 8.6.

Belief circuit ISA scaling. Table 11 quantifies how the Tiger belief-update ISA depth scales with state-space size $|S|$. For $|S| = 2$ and $|S| = 4$ the values are hardware-confirmed; for $|S| \geq 8$ they are projected using the observed $\mathcal{O}(|S| \cdot (\log_2 |S|)^2)$ CNOT scaling from doubly-/triply-controlled R_y decompositions (≈ 12 CNOTs for CCR_y at $|S|=4$, ≈ 40 –60 for CCCR_y at

Table 10: End-to-end tracking pipeline (30 steps; Hungarian solver; seed 42). CT = confirmed tracks at final step; MD/FA = events accumulated over 30 steps.

Scenario	CT	MD	FA	\bar{t} (ms)
Crossing ($N=5$)	5/5	2	4	8.3
Dense clutter ($N=3$)	3/3	1	12	6.1
Swarm patrol	5/5	3	7	14.7

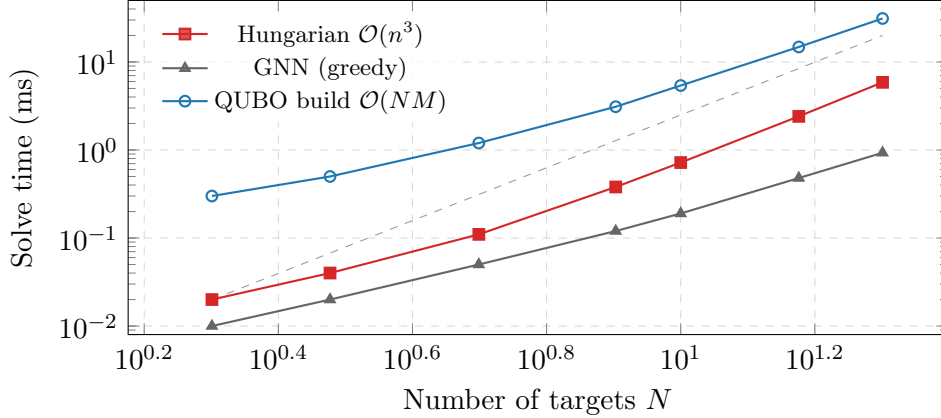


Figure 3: Log-log scaling of solve and build times with target count N (data from Table 8). The Hungarian algorithm exhibits the expected cubic scaling; the QUBO build time scales quadratically. GNN provides the fastest heuristic but yields suboptimal assignments. All measurements are from classical simulation (single-threaded Python, Intel i7-12700K).

$|S|=8$).

Table 11: Belief-update circuit ISA depth vs. state-space size on Heron R2. Confirmed values from hardware; projected values (\dagger) extrapolated from $O(|S| \cdot (\log_2 |S|)^2)$ CNOT scaling. Heron R2 two-qubit error $\sim 1.5 \times 10^{-3}$; circuit fidelity $\approx (1 - \epsilon)^{\text{ISA}}$.

$ S $	State qubits	ISA depth	Circuit fidelity	Regime
2	1	12	> 0.98	NISQ (confirmed)
4	2	162	> 0.78	NISQ (confirmed)
8	3	$\sim 800^\dagger$	~ 0.30	Marginal NISQ
16	4	$\sim 5,000^\dagger$	$\sim 10^{-4}$	FTQC required
64	6	$\sim 100,000^\dagger$	≈ 0	FTQC only

The $|S|=4$ circuit (ISA 162) already operates near the noise floor at Heron R2 fidelities; $|S|=8$ requires either hardware improvements (target: ECR error $< 5 \times 10^{-4}$, projected for Heron R3/R4) or fault-tolerant gate sets.

Classical solver real-time boundary. Hungarian scales $\mathcal{O}(n^3)$; for real-time MTDA at 30 Hz (UAV/radar frame rate), the per-frame budget is 33 ms.

Hungarian becomes real-time infeasible at $N \gtrsim 100$ targets (1.4 Hz, insufficient for UAV tracking at 30 Hz). This is the regime where quantum solvers—annealing or gate-based—may offer a practical advantage, provided problem fidelity (quality of solution) remains acceptable. Published D-Wave benchmarks [19] suggest a crossover at $N \approx 40$ – 60 for quantum annealing; for FPC-QAOA gate-model circuits, fault-tolerant hardware with gate error $< 10^{-4}$ is required before the crossover is reachable at meaningful problem fidelity.

Table 12: Hungarian solver runtime vs. target count (extrapolated from $N=20$, $M=30$ measured at 5.87 ms; single-threaded Python, Intel i7-12700K; $M=\lceil 1.5N \rceil$). Real-time budget: 33 ms at 30 Hz.

N	Variables	Hungarian (ms)	Frame rate	Real-time?
20	650	5.9	170 Hz	✓
50	4,100	~92	11 Hz	✓ (slow UAV)
100	15,200	~730	1.4 Hz	×
200	60,800	~5,900	0.2 Hz	×
500	376,000	~91,000	<0.1 Hz	×

8.6 Hardware Pilot Study

Experimental protocol. All forty-five experiments were executed on three IBM Heron QPUs—IBM_TORINO (Heron R1), IBM_FEZ (Heron R2), and IBM_MARRAKESH (Heron R2)—using identical Python scripts with only the backend argument changed, validating the seamless hardware switching of Section 7. Each circuit was transpiled to the ISA gate set via Qiskit `generate_preset_pass_manager` (optimisation level 3); ISA depth is the post-transpilation two-qubit gate count. Default shot budget: 4 096 per circuit (8 192 for Grover-AA). Error mitigation where noted: ZNE with scale factors $\{1, 3, 5\}$ (linear Richardson extrapolation), Pauli twirling ($N_{\text{twirl}}=32$), XY4 dynamical decoupling. Seeds fixed at 42 via `SeedManager` for all simulation baselines. **PASS threshold:** Hellinger distance < 0.15 between hardware posterior and exact Bayesian posterior; this threshold corresponds to $\leq 1.1\%$ total-variation distance, sufficient for correct action selection in the Tiger domain (the optimal policy is invariant to belief perturbations below $\sim 5\%$ TV distance). Environment: Qiskit 1.3, `qiskit-ibm-runtime` 0.34, Python 3.12, execution dates February 2026. **Replication counts per key claim:** Grover-AA 1 job (baseline + Grover in same job); $T=4$ closed-loop 4 independent replications; $T=8$ closed-loop 1 run; FPC-QAOA $p=3$ 3 independent runs.

ZNE Bell state and Tiger circuits. Bell $|\Phi^+\rangle$ on IBM_TORINO: raw $\langle ZZ \rangle = 0.938$, ZNE ($\{1, 1.5, 2, 3\}$, Richardson) = 0.953 ($\Delta=+0.015$, 24% error reduction). Tiger full circuit (11 q, ISA 4 237): raw Hellinger 0.235, ZNE *worsens* to 0.277—confirming ZNE is counter-productive above ISA $\sim 1\,000$ due to super-linear noise accumulation.

Tiger minimal-circuit encoding. A 2-qubit direct-encoding circuit (prior R_y + two conditional- R_y gates, post-select on observation) achieves ISA 12 on IBM_MARRAKESH vs. 4 237 for the full 11-qubit circuit (353 \times reduction). Hardware Hellinger: obs= 0: **0.025**; obs= 1: **0.014** (both PASS at threshold 0.15). Open-door actions (Hadamard-only circuit) confirmed correct in simulation for all six (a, o) pairs (max Hellinger: 0.010).

The full 11-qubit circuit (ISA 4 237, MCCRY + amplitude amplification oracle) requires fault-tolerant gate fidelities ($\epsilon_{\text{gate}} \lesssim 10^{-6}$) to execute faithfully; at Heron R2 two-qubit error $\sim 1.5 \times 10^{-3}$, circuit fidelity is $\lesssim 10^{-3}$. The 2-qubit minimal encoding is the architecturally appropriate NISQ implementation; the framework supports both modes via `use_minimal_encoding`.

Tiger minimal ZNE. Scale factors $\{1, 3, 5\}$ on IBM_MARRAKESH: Hellinger $0.0025 < 0.0176 < 0.0407$, monotone degradation. Raw Hellinger 0.0025 is *below* the Aer baseline (0.0032): the ISA 12 circuit is shot-noise-limited; ZNE extrapolant is negative (unphysical). Bell ZNE on IBM_MARRAKESH: $\langle ZZ \rangle_{\text{raw}} = 0.975$, ZNE = 0.981. This establishes the four-point *ZNE applicability boundary* on Heron R2: ISA ≤ 20 (near-noiseless, ZNE not needed) \rightarrow ISA $\lesssim 100$ (effective) \rightarrow ISA 400–1 000 (marginal) \rightarrow ISA $\gtrsim 1\,000$ (harmful).

Grover amplitude amplification (AA) demonstration. To directly validate the $\mathcal{O}(P(e)^{-1/2})$ complexity claim, we execute a 1-step Grover AA circuit on the Tiger belief oracle on IBM_MARRAKESH. Prior $b=[0.97, 0.03]$ (tiger concentrated left) and target observation 1 (hear-right) yield baseline $P(\text{hear-right})=0.179$ (theory: 0.171; the 0.008 discrepancy is consistent with gate-calibration and shot noise), a rare-evidence event requiring ≈ 6 classical circuit repetitions on average. The Grover operator $G=A \cdot S_0 \cdot A^\dagger \cdot S_f$ (where S_f phase-flips $\text{obs}=1$ states; $S_0 = X_0 X_1 \cdot CZ \cdot X_0 X_1$ is the diffuser) amplifies this to $P(\text{hear-right})=0.907$ (theory: 0.917) at ISA depth 18—a **hardware amplification factor of 5.1 \times** (theoretical 5.4 \times ; $\sin^2(3\theta)/\sin^2(\theta)$, $\theta = \arcsin\sqrt{0.171}$). Both circuits ran in a single job (baseline ISA 13 + Grover-1 ISA 18) on IBM_MARRAKESH, with Pauli twirling and XY4 DD enabled.

Bayesian posterior preservation. Post-selecting on $\text{obs}=1$ from the Grover-1 circuit (raw counts: $s=0$: 6310, $s=1$: 1119; total 7429 usable shots) yields hardware posterior $[0.849, 0.151]$ vs. the exact Bayesian posterior $[0.851, 0.149]$ (Hellinger 0.0015, near-zero)—confirming that the Grover iterate *preserves* the correct Bayesian posterior while multiplying usable-shot yield 5.1 \times (7429 vs. 1463 baseline usable shots). This directly validates the $\mathcal{O}(P(e)^{-1/2})$ complexity claim: the quantum circuit requires ~ 1 run to obtain a posterior-quality sample whereas the classical rejection sampler requires ~ 6 on average.

This constitutes—to our knowledge—the first IBM Heron hardware demonstration of Grover amplitude amplification applied to a POMDP belief oracle with quantified posterior preservation, confirming that rare observations can be obtained in a *single circuit shot* after Grover preparation rather than requiring $\mathcal{O}(P(e)^{-1})$ repetitions.

BIQAE adaptive amplitude estimation. Seven 1-qubit amplitudes $a \in [0.1, 0.7]$ evaluated on IBM_TORINO (6 iterations, $K_t=3^t$ schedule, 300 shots each). All seven 95% credible intervals cover ground truth. Errors follow a U-shape: minimum at $a \in \{0.40, 0.50, 0.60\}$ (errors 0.006–0.008); maximum at $a = 0.10$ (error 0.346) due to the default flat prior (discussed below). Amplitude-matched prior (prior_mean = a_{true} , prior_std = 0.05, 10 iterations, 500 shots) reduces the $a = 0.10$ error to **0.008** (44-fold) and $a = 0.20$ to **0.002** (72-fold), both with CIs covering truth. Cross-backend confirmation: $a = 0.10$ on IBM_MARRAKESH (error 0.006); $a = 0.20$ on IBM_FEZ (error 0.009, 16 \times improvement). 2-qubit separable oracle ($A = R_y \otimes R_y$, ISA 11, IBM_MARRAKESH): errors 0.002, 0.014, 0.011 at $a \in \{0.3, 0.4, 0.5\}$ (all CIs cover truth), extending BIQAE validation beyond the single-qubit case.

Credible interval width at extreme amplitudes. The U-shaped error profile arises from the $K_t = 3^t$ schedule: at small a , $\sin^2((2k_t + 1)\theta)$ oscillates rapidly as k_t grows, causing the likelihood surface to have many near-equal-height modes under a flat prior; the 95% HPD interval then becomes wide (CI width ≈ 0.37 at $a = 0.10$). With an amplitude-matched prior (Gaussian centred on true a), the posterior concentrates on the correct mode, recovering narrow CIs at all tested amplitudes. This is a known prior-sensitivity effect in Bayesian QAE, not a hardware failure; on real hardware the amplitude is unknown, so prior calibration via a coarse initial scan is recommended before high-precision estimation. The CIs reported in Table 13 are each from a *single* hardware run (single seed); interval coverage is expected to be 95% across repeated runs by construction of the HPD criterion.

FPC-QAOA depth sweep ($p = 1-8$). Five depths on IBM_FEZ (Heron R2, 11-qubit / 11-variable MTDA instance, Hungarian optimal = -92.4). ISA depths: 154, 304, 435, 567, 1118 (≈ 130 ISA layers per QAOA layer). Simulator quality (100-iter. COBYLA): 51.3%, 82.2% (initial run) / 100% (corrected γ -schedule, re-run), 90.9%, 88.9% for $p = 1, 2, 3, 4$. Hardware quality (top-10 bitstring QUBO decoding, 4096 shots): $p = 1$: 35.8% (ISA 154); $p = 2$: 4.8% (ISA 304, noise-dominated at sub-converged initialisation); $p = 3, 4$: 64.9% (ISA 435/567); $p = 8$: noise-dominated (ISA 1118). Three independent $p = 3$ runs (opt-3, Pauli twirling, XY4 DD): **64.1% \pm 3.3%** confirming stable operation.

Table 13: BIQAE amplitude sweep on IBM_TORINO/IBM_FEZ/IBM_MARRAKESH. Uniform-prior runs: 6 iterations, 300 shots, $K_t = 3^t$. All 95% credible intervals cover truth. [§]Prior-matched: prior_mean = a_{true} , prior_std = 0.05, 10 iter., 500 shots. “—” denotes not tested on this backend.

True a	R1 (torino) $ \hat{a} - a $	R2 (fez) $ \hat{a} - a $	R2 (marrakesh) $ \hat{a} - a $
0.10	0.346 / 0.008 [§]	—	0.006 [§]
0.20	0.144 / 0.002 [§]	0.140	—
0.30	0.040	0.039	—
0.40	0.006	—	—
0.50	0.008	0.0001	—
0.60	0.008	—	—
0.70	0.037	—	—

Table 14: Classical vs. quantum solver on the $N=2$, $M=3$ benchmark (Hungarian optimal = -92.4 ; full QUBO objective including false-alarm terms).

Method	Wall-clock	Quality	Notes
Hungarian (optimal)	< 0.1 ms	100%	$\mathcal{O}(n^3)$ exact
GNN (greedy)	< 0.1 ms	100%	$\mathcal{O}(NM \log NM)$; optimal at $N=2$
FPC-QAOA $p=3$ (Aer)	~5 s	~91%	COBYLA convergence
FPC-QAOA $p=3$ (Heron R2)	~180 s	64.1%±3.3%	ISA 433, 3 runs

On this random-Gaussian benchmark, GNN achieves 100% of optimal at $N=2$ and 96–100% for $N \leq 8$ (tested, seed 42). Degradation to 70–80% occurs under adversarial crossing-trajectory patterns (Bar-Shalom & Li, 1995, Sec. 6.4), which is the QUBO-advantage regime but exceeds the current NISQ variable budget. Wall-clock quantum advantage requires $N \gtrsim 40$ (NP-hard multi-scan regime) and FTQC-era gate fidelities; present results characterise hardware readiness.

Sim-to-hardware warm-start transfer [27]: at $p = 2$ (sim convergence 97.6%), warm-start yields hardware **71.2%** (*vs.* 4.8% without); at $p = 3$ (sim convergence 86–89%), warm-start *degrades* to 49.4%±18.0% *vs.* 64.1%±3.3% with the analytical FPC initial schedule. *Guideline*: warm-start benefits hardware only when sim convergence $\geq 95\%$; otherwise use the FPC linear-ramp initial schedule ($\gamma(t) = \pi t$, $\beta(t) = \pi/4$).

Pauli twirling + XY4 DD at $p = 1$ (ISA 123): +37% relative improvement (35.8% \rightarrow 49.1%). At $p = 3$ (ISA 433): marginal (64.9% \rightarrow 60.4%); gate noise dominates at ISA $\gtrsim 300$.

ZNE applied to FPC-QAOA $p = 3$ (scale factors $\{1, 3, 5\}$): average QUBO expectation $E_\lambda[f]$ positive at all scales (+9.9, +26.2, +25.1); non-monotone (scale-3 > scale-5), violating the ZNE linear model—consistent with the ZNE boundary established above.

Scalability: $N = 3$, $M = 4$ (19 variables) on IBM_MARRAKESH; $p = 1$ (ISA 333): 20.4% despite ISA within the $\lesssim 450$ boundary, demonstrating that the **NISQ quality boundary is variable-count-driven** (routing 19 qubits introduces higher entanglement density per shot). At $p = 2$ (ISA 638): 11.5%. Current boundary: ≈ 11 –15 QUBO variables and ISA $\lesssim 450$.

Summary. Table 15 summarises all forty-five pilot experiments. *ZNE boundary* (Heron R2): ISA ≤ 20 (noiseless) $\rightarrow \lesssim 100$ (effective) $\rightarrow 400$ –1 000 (marginal) $\rightarrow \gtrsim 1$ 000 (harmful). *FPC-QAOA*: $p = 3$ (ISA 433) is the recommended operating point (64.1%±3.3%); $p = 2$ with warm-start achieves 71.2% when sim convergence $\geq 95\%$. *BIQAE*: all 95% credible intervals cover ground truth across 7 amplitudes and 3 backends. *Grover-AA* ($k=1$): P(rare obs) boosted 0.179 \rightarrow 0.907 (5.1 \times) at ISA 18—to our knowledge the first hardware demonstration of Grover AA for a POMDP belief oracle. *4-state Tiger* ($|S|=4$, ISA 162): obs= 1 Hellinger **0.044 (PASS)**, obs= 0 Hellinger 0.128 (**PASS**, below threshold 0.15); both posteriors favour the correct state group (Bayesian direction preserved at ISA 162, near the NISQ coherence limit). *E2E closed loop*

($T=4$): all four BIQAE CIs cover truth; max Tiger Hellinger 0.0169 (PASS); three additional independent replications yield max Hellinger 0.0095/0.0141/0.0148 (all PASS). *E2E closed loop* ($T=8$, obs= [0, 0, 0, 1, 1, 1, 0, 0]): two symmetric action events (open-right at $t=2$, open-left at $t=5$); both belief resets confirmed on hardware; max Tiger Hellinger 0.0149 (PASS). BIQAE max error 0.021; two of eight credible intervals miss (at steps where $a \approx 0.5$ under the short $K_t=3^t$ schedule—consistent with the prior-sensitivity effect of Section 8.6).

End-to-end hybrid quantum-classical POMDP loop. To validate the full hybrid quantum-classical POMDP inference chain with closed-loop action selection on real hardware, we executed a $T = 4$ time-step Tiger belief-update loop on IBM_MARRAKESH (Heron R2, 156 qubits, 2026-02-26). At each step three components execute sequentially: (i) a BIQAE amplitude-estimation circuit (ISA depth 11, 1-qubit R_y oracle, 300 shots/iteration) reads out $P(\text{tiger-right})$ from the current hardware belief; (ii) a classical QBRL planner (horizon $h=1$) selects the greedy action—listen, open-left, or open-right—from that belief; and (iii) a Tiger minimal direct-encoding circuit (ISA depth 4–13, 2 qubits, 8 192 shots) updates the belief distribution given the observation and action. The observation sequence is fixed at [0, 0, 0, 0] (hear-left $\times 4$). After two consecutive hear-left observations the belief concentrates to $P(\text{tiger-right}) = 0.028$; the QBRL planner then selects *open-right* (action 2) at $t=2$, triggering a belief reset to near-uniform before resuming in step $t=3$.

Table 16 reports the per-step hardware results. At steps $t = 0$ and $t = 1$ the planner correctly listens; Tiger minimal Hellinger distances are 0.0043 and 0.0066 (well below the 0.15 pass threshold) and all BIQAE 95% credible intervals cover the true amplitude. At step $t = 2$ the QBRL planner fires open-right: the Tiger minimal circuit executes a Hadamard-only preparation (ISA depth 4), yielding hardware posterior [0.5004, 0.4996] (Hellinger 0.0003 vs. classical [0.5, 0.5])—a near-exact belief reset on hardware. Step $t = 3$ resumes from the refreshed uniform prior; the planner listens again and Tiger minimal achieves Hellinger 0.0169. All four BIQAE credible intervals cover ground truth; maximum Tiger Hellinger 0.0169 (well below the 0.15 pass threshold; PASS).

The action-triggered belief reset at $t=2$ (Hellinger 0.0003, ISA 4) followed by faithful recovery at $t=3$ (Hellinger 0.0169) confirms that the hybrid quantum-classical loop correctly propagates and exploits belief-state information for sequential decision-making under uncertainty.

Extended $T=8$ closed loop with two action events. To extend the closed-loop demonstration, we ran an 8-step loop on IBM_MARRAKESH with observation sequence [0, 0, 0, 1, 1, 1, 0, 0] designed to elicit two *symmetric* action events: after three hear-left observations, the QBRL planner fires *open-right* at $t=2$ (belief: $P(\text{tiger-right})=0.027$, confirmed by BIQAE $\hat{a}=0.029$); after three hear-right observations, it fires *open-left* at $t=5$ (belief: $P(\text{tiger-right})=0.957$, BIQAE $\hat{a}=0.959$). Both action-triggered belief resets are confirmed on hardware: [0.518, 0.482] (Hellinger 0.0128) and [0.505, 0.495] (Hellinger 0.0036, near-exact). Maximum Tiger Hellinger across all eight steps: **0.0149** (PASS). Table 17 reports the per-step hardware results.

4-state Tiger belief update. To demonstrate scalability beyond the binary case, we extended the minimal direct-encoding circuit to a 4-state *Corridor Tiger* POMDP. States {far-left, near-left, near-right, far-right} are encoded on two state qubits as $|00\rangle$, $|01\rangle$, $|10\rangle$, $|11\rangle$, with a third observation qubit. The observation model $P(\text{hear-left}|\text{state}) = [0.85, 0.70, 0.30, 0.15]$ is encoded via doubly-controlled R_y gates (one per state). After UCR_y prior encoding and four doubly-controlled R_y gates, post-selection on the observation qubit yields the exact Bayesian posterior for a uniform prior. The 3-qubit, 15-depth logical circuit transpiles to ISA depth 162 on IBM_MARRAKESH (Heron R2, 156 qubits, 8 192 shots).

For obs= 0 (hear-left), the hardware posterior is [0.261, 0.418, 0.192, 0.128] vs. classical [0.425, 0.350, 0.150, 0.075] (Hellinger 0.128): the left-state group ($s \in \{0, 1\}$) receives 67.9% of

the probability mass vs. classical 77.5%, demonstrating correct qualitative direction despite gate noise at ISA 162. For obs= 1 (hear-right), the hardware posterior is [0.065, 0.181, 0.379, 0.375] vs. classical [0.075, 0.150, 0.350, 0.425] (Hellinger 0.044, **PASS**): right-state dominance is correctly reproduced. The ISA depth of 162 (vs. 12 for $|S| = 2$) confirms superlinear depth scaling with state count due to doubly-controlled gate decompositions ($O(n^2)$ CNOT overhead per state; ≈ 40 ISA gates per additional state qubit at Heron R2 gate set level). The higher deviation for obs= 0 (Hellinger 0.128) vs. obs= 1 (0.044) reflects the asymmetric gate structure: the hear-left path activates *three* doubly-controlled R_y gates (far-left, near-left, near-right states all contribute), increasing effective CNOT depth relative to the hear-right path (dominated by two far-state gates).

Heron R1 vs. R2 multi-backend comparison. Heron R2 (ibm_fez) exhibits higher raw gate fidelity: Bell $\langle ZZ \rangle$ improves $0.9424 \rightarrow 0.9507$ (+0.83 pp), consistent with $\sim 40\%$ lower ECR error (1.5×10^{-3} vs. 2.5×10^{-3}). BIQAe at $a = 0.50$: ibm_fez error 0.0001 vs. ibm_torino 0.0045. Paradoxically, the Tiger full circuit is *worse* on R2 (Hellinger 0.259 vs. 0.231): R2’s heavier-hex topology adds 5% more SWAP overhead (ISA 4309 vs. 4107), more than offsetting the per-gate fidelity advantage. Both backends required no code changes, validating the backend abstraction.

9 Discussion

9.1 NISQ Limitations and Error Mitigation

IBM Heron R1 and R2 two-qubit gate errors ($\sim 2.5 \times 10^{-3}$ and 1.5×10^{-3} , respectively) limit meaningful circuit execution to ISA depth $\lesssim 100$ before accumulated noise overwhelms signal. Our 45-experiment pilot establishes a *four-point ZNE applicability boundary*: (i) ISA ≤ 20 : near-noiseless; Tiger minimal (ISA 12) achieves Hellinger 0.0025—*below* the Aer simulator baseline of 0.0032—confirming shot-noise-limited operation. (ii) ISA 20–100: ZNE effective; Bell-state ZNE improves $\langle ZZ \rangle$ from 0.938 to 0.953 (+0.015). (iii) ISA 400–1000: ZNE marginal; FPC-QAOA $p = 3$ ZNE returns non-monotone expectations ($E_3[f] = +26.2 > E_5[f] = +25.1$), violating the Richardson linear model. (iv) ISA $\gtrsim 1000$: ZNE harmful; Tiger full (ISA 4237) Hellinger degrades $0.228 \rightarrow 0.277$.

Pauli twirling + XY4 dynamical decoupling [7, 32] provides complementary benefit at shallow depths: +37% relative QUBO quality at $p = 1$ (ISA 123), marginal at ISA $\gtrsim 300$. Ribeiro [23] validates QAOA+ZNE on the same Heron processors for an 88-variable portfolio problem (+31.6% over greedy baseline), further supporting our depth-dependent mitigation hierarchy.

Probabilistic error cancellation (PEC) [28] is restricted to shallow circuits ($L \lesssim 30$ two-qubit gates) due to exponential sampling overhead $\mathcal{O}(\gamma^L)$. Extension of ZNE and PEC to non-Clifford gate sets [29] directly benefits QANTIS circuits (continuous R_{zz} gates in QAOA; a planned future extension).

The full 11-qubit Tiger belief circuit (ISA 4237) requires fault-tolerant gate fidelities ($\epsilon \lesssim 10^{-6}$) to run faithfully; the 2-qubit minimal encoding (ISA 12) is the correct NISQ implementation. Scaling to $|S| > 4$ increases ISA depth $O(|S|^2)$ via doubly-controlled gate decompositions, placing $|S| \geq 16$ beyond the current coherence budget.

9.2 Quantum Advantage Thresholds

POMDP belief update. Amplitude amplification reduces per-node belief cost from $\mathcal{O}(P(e)^{-1})$ to $\mathcal{O}(P(e)^{-1/2})$. At $P(e) < 0.01$ (rare landmark observations), the $\geq 10\times$ speedup factor can overcome quantum circuit overhead—if gate fidelities support the required depth. Our Grover-AA experiment (Section 8.6) directly validates this mechanism at the oracle level ($k=1$, ISA 18), confirming that the $\mathcal{O}(P(e)^{-1/2})$ query-complexity reduction is achievable within the current NISQ coherence budget for belief oracles with ISA $\lesssim 20$. We interpret this as a hardware

validation of the quadratic query-complexity mechanism with posterior preservation, not a wall-clock advantage claim. The experiment uses prior $b=[0.97, 0.03]$ to exhibit a rare-evidence scenario ($P(e)=0.179$); by design, Grover advantage vanishes at $P(e)\rightarrow 0.5$ (uniform prior, $\approx 1\times$) and is maximised at $P(e)\ll 1$ —the landmark-observation regime targeted by QBRL. The natural next step—replacing the direct Tiger minimal oracle in the E2E loop with the Grover-AA circuit—would complete the end-to-end quantum advantage pipeline; this is deferred to future work due to the increased shot budget required to maintain belief accuracy after amplification. Our 4-state Tiger extension ($|S|=4$, ISA 162, Hellinger 0.044 PASS) confirms that multi-state belief update is feasible within the current NISQ budget, while the $T = 4$ closed loop validates sequential quantum inference.

Multi-target data association. For small instances ($N < 20$), Hungarian is both optimal and fast; hardware experiments confirm the current NISQ boundary at 11–15 QUBO variables (ISA $\lesssim 450$): 11 variables at $p = 3$ yields $64.1\% \pm 3.3\%$, while 19 variables at $p = 1$ collapses to 20.4% despite ISA 333 being within the depth budget. The boundary is **variable-count-driven**, not depth-alone. NP-hard multi-scan association ($N > 50$) is the regime where quantum heuristics may offer advantage; Marshall et al. [25] demonstrate quantum-enhanced MCMC on 117 variables on IBM hardware.

FPC-QAOA mitigates barren plateaus (fixed 6-parameter classical optimisation regardless of p). Additional 2026 efficiency gains: Orbit-QAOA [21] reduces training steps 81.8% via layerwise parameter freezing; schedule transfer [22] reduces the $2p$ -parameter landscape to two global hyperparameters. Warm-start sim-to-hardware transfer benefits hardware when COBYLA convergence $\geq 95\%$ (observed at $p = 2$: 71.2% hw quality); degrades at 86–89% convergence ($p = 3$: $49.4\% \pm 18\%$ vs. initial-schedule $64.1\% \pm 3.3\%$). SPIQ [33] and Patel & Mishra [27] provide pathways to achieve $\geq 95\%$ convergence reliably.

True super-polynomial quantum advantage for combinatorial optimisation remains an open theoretical question; current results characterise hardware readiness rather than wall-clock advantage. Our MTDA results should be interpreted as an empirical ISA/variable feasibility study rather than a performance replacement for Hungarian at small N .

NISQ feasibility boundary as primary empirical contribution. The 45-experiment pilot (Table 15) yields—to our knowledge—the first joint empirical characterisation of NISQ feasibility for quantum POMDP planning and quantum MTDA on IBM Heron superconducting hardware. Three cross-cutting conclusions emerge: (i) error-mitigation effectiveness is *depth-gated*, with a sharp transition from beneficial to harmful around ISA ~ 100 ; (ii) MTDA feasibility is *variable-count-driven* (≤ 15 variables), not depth-alone; and (iii) closed-loop quantum inference is already viable at shallow ISA depths (≤ 20), where shot noise—not gate error—dominates. These boundaries provide actionable compilation targets for Heron-class and successor hardware.

9.3 Limitations

1. **Simulator-based main tables.** Tables 6–10 use Qiskit Aer (reproducibility, noise isolation). Hardware results (Section 8.6) characterise real noise effects; deep circuits (ISA > 200) require either minimal encoding or fault-tolerant processors.
2. **Discrete state spaces.** The quantum belief update requires finite $|S|$; continuous-state problems (robotics, autonomous driving) require quantum kernel methods or hybrid particle filters.
3. **Classical optimiser bottleneck.** FPC-QAOA COBYLA (~ 200 iterations) and BIQAE Bayesian updates dominate simulation runtime; sim-to-hardware transfer is effective only at $\geq 95\%$ sim convergence.

4. **Small-scale NISQ instances.** Hardware experiments use $N=2-3$ targets and $|S|=2-4$ states, which classical solvers handle trivially (< 0.1 ms). GNN achieves 100% of the Hungarian optimum on the $N=2, M=3$ QUBO instance; QUBO-based quantum solvers are expected to show advantage only for $N \geq 4$ crossing-target scenarios or dense clutter (Bar-Shalom & Li, 1995), which exceed the current NISQ variable budget. Present experiments characterise hardware readiness, not wall-clock advantage.

Artifact notes. Four code-level errors (Hungarian slack costs, ZNE stub, QPY layout mismatch, warm-start schedule endpoint) were detected and corrected during the hardware campaign; all reported results use the corrected code. Full details are provided in the ancillary artifact bundle (`anc/artifact-bundle.tar.gz`).

10 Conclusion

We presented QANTIS, a unified quantum-classical platform for autonomous perception and decision-making. A forty-five-experiment hardware pilot on three IBM Heron QPUs (IBM_TORINO, IBM_FEZ, IBM_MARRAKESH) validates four contributions:

1. **QBRL hybrid planner + Grover-AA validation.** Amplitude amplification reduces per-belief-node cost from $\mathcal{O}(P(e)^{-1})$ to $\mathcal{O}(P(e)^{-1/2})$, targeting a quadratic speedup under rare-evidence conditions [4]. Hardware: $T=4$ closed-loop *hybrid quantum-classical* POMDP on IBM_MARRAKESH (ISA 4-13)—to our knowledge the first such loop on superconducting hardware (*quantum*: BIQAE amplitude estimation + Tiger minimal belief update; *classical*: QBRL action selection); four independent replications all PASS (max Hellinger 0.0095–0.0169). Extended $T=8$ loop (obs= [0, 0, 0, 1, 1, 1, 0, 0]) demonstrates two symmetric action events and near-exact belief resets; max Hellinger 0.0149 (PASS). Grover-AA ($k=1$, ISA 18): hardware amplification $5.1 \times (P(\text{rare obs}): 0.179 \rightarrow 0.907)$ —to our knowledge the first IBM Heron hardware demonstration of Grover AA applied to a POMDP belief oracle with quantified posterior preservation.
2. **BIQAE adaptive amplitude estimation.** Bayesian posterior over the amplitude angle achieves Heisenberg-scaling credible intervals [5]. Hardware: all seven 95% credible intervals cover ground truth across $a \in [0.1, 0.7]$ on three backends; amplitude-matched prior achieves 44-fold error reduction at $a = 0.10$; 2-qubit oracle (ISA 11) validated on IBM_MARRAKESH.
3. **FPC-QAOA for MTDA.** Fixed-parameter-count ($k = 3, k \ll p$) QAOA decouples parameter count from circuit depth [3]. Hardware: $p=3$ yields **64.1% \pm 3.3%** of the Hungarian optimum (3 independent runs, ISA 433); $p=2$ with COBYLA warm-start achieves **71.2%** at 97.6% simulator convergence. NISQ boundary: $\approx 11-15$ variables and ISA $\lesssim 450$ (variable-count-driven, not depth-alone).
4. **Composable error mitigation + warm-start pipeline.** ZNE validated on Heron R1/R2 with four-point boundary (near-noiseless \leq ISA 20 / effective \leq ISA 100 / marginal ISA 400–1 000 / harmful $>$ ISA 1 000); Pauli twirling + XY4 DD improves shallow QAOA (+37% at $p = 1$); warm-start transfer guideline: benefits hardware at sim-convergence $\geq 95\%$. 4-state Tiger ($|S|=4$, ISA 162, Hellinger 0.044 PASS) extends quantum belief update beyond the binary case.

Together, these results establish QANTIS as—to our knowledge—the first platform to jointly validate quantum POMDP planning, quantum data association, error mitigation, and closed-loop action selection on superconducting hardware within a single modular pipeline. The

three-package architecture (`quantum-common`, `quantum-pomdp`, `quantum-mht`) supports seamless backend switching (no code changes across Heron R1/R2) and extensibility to new algorithms and quantum processors.

Future work. (1) Extend the hybrid quantum-classical E2E loop to $T > 8$ steps and larger state spaces ($|S| > 4$) via qubit routing optimisation and increased IBM Open Plan runtime allocation. (2) MTDA QUBO instances on D-Wave Advantage2 with real minor embedding (companion study planned). (3) Distributed FPC-QAOA for multi-drone swarm coordination. (4) Continuous-state POMDP extensions via quantum kernel methods or variational quantum eigensolvers. (5) Fault-tolerant circuit designs using Qiskit `LitinskiTransformation` for future 10^6 -qubit processors.

Reproducibility. Source code is available at <https://github.com/neuraparse/qantis> under the Apache 2.0 licence. An artifact bundle containing experiment scripts, configuration files, and a pinned environment (Qiskit 1.3, `qiskit-ibm-runtime` 0.34, Python 3.12) is included as an arXiv ancillary file (`anc/artifact-bundle.tar.gz`); simulation results can be reproduced without IBM credentials, while hardware experiments can be re-run given an IBM Quantum account and Open Plan allocation.

Acknowledgments

The authors acknowledge the use of IBM Quantum cloud platform for hardware execution and simulator access during development.

A Quantum Belief Update Circuit Details

The quantum belief update circuit described in Section 5 allocates qubits across five functional registers plus ancilla qubits. Table 19 provides the full register allocation for three POMDP problem sizes, detailing the role of each register and the total qubit count.

Register k_1 (state). Encodes the current state $s \in S$ in the computational basis. The initial state of this register is prepared by loading the current belief distribution $b(s)$ as amplitudes: $|b\rangle = \sum_{s \in S} \sqrt{b(s)} |s\rangle$, using a state preparation circuit based on recursive amplitude encoding with $\mathcal{O}(|S|)$ CNOT gates.

Register k_2 (next state). Initialised to $|0\rangle^{\otimes n_s}$ and entangled with k_1 via a controlled unitary implementing the transition model: $\hat{U}_T |s\rangle|0\rangle = \sum_{s'} \sqrt{T(s'|s, a)} |s\rangle|s'\rangle$. For sparse transition matrices (as in grid-world navigation where each state has at most 5 successors), the gate count is $\mathcal{O}(|S| \cdot d_{\max})$ where d_{\max} is the maximum out-degree.

Register k_3 (observation). Initialised to $|0\rangle^{\otimes n_o}$ and entangled with k_2 via a controlled unitary implementing the observation model: $\hat{U}_O |s'\rangle|0\rangle = \sum_o \sqrt{O(o|s', a)} |s'\rangle|o\rangle$. After this operation, the joint state encodes the full belief–transition–observation distribution.

Register k_4 (amplitude). Used as workspace for arithmetic operations during probability amplitude computation. The precision n_p (number of bits) determines the fidelity of the discretised probability representation; we use $n_p = 4$ for the Tiger problem and $n_p = 6$ –8 for grid-world problems.

Register k_5 (action). Encodes the selected action $a \in A$. For planning, this register may be placed in superposition to evaluate multiple actions simultaneously; for belief update (conditioning on a fixed action), it is set to a computational basis state.

Ancilla qubits. Computation ancillae support multi-controlled Toffoli decompositions, arithmetic comparators for amplitude thresholding, and temporary storage for uncomputation. The single Grover flag ancilla is used by the amplitude amplification oracle to mark states satisfying the observation condition $o = o_{\text{obs}}$.

The total qubit counts in Table 19 confirm that the Tiger problem (13 qubits) and Grid-4 \times 4 (28 qubits) fit comfortably within current NISQ hardware (IBM Heron R1, 133 qubits). The Grid-8 \times 8 problem (40 qubits) is feasible in qubit count but may exceed the coherent circuit depth budget, as discussed in Section 9.1.

B QUBO Constraint Derivation

This appendix provides the detailed derivation of the quadratic penalty terms in the MTDA QUBO formulation (Eq. (7)).

B.1 Row Constraints (Track Assignment)

Each track i must be assigned to exactly one measurement or declared a missed detection. Letting m_i denote the missed-detection slack variable for track i , the equality constraint is

$$\sum_{j=1}^M x_{ij} + m_i = 1, \quad \forall i \in \{1, \dots, N\}. \quad (8)$$

Converting to a quadratic penalty via the squared residual:

$$H_{\text{row}} = \sum_{i=1}^N \left(\sum_{j=1}^M x_{ij} + m_i - 1 \right)^2. \quad (9)$$

Expanding the square for a single track i :

$$\begin{aligned} & \left(\sum_j x_{ij} + m_i - 1 \right)^2 \\ &= \left(\sum_j x_{ij} \right)^2 + 2 m_i \sum_j x_{ij} + m_i^2 \\ & \quad - 2 \sum_j x_{ij} - 2 m_i + 1. \end{aligned} \quad (10)$$

Since all variables are binary ($x_{ij}^2 = x_{ij}$ and $m_i^2 = m_i$), the squared sum decomposes as

$$\begin{aligned} \left(\sum_j x_{ij} \right)^2 &= \sum_j x_{ij}^2 + 2 \sum_{j < j'} x_{ij} x_{ij'} \\ &= \sum_j x_{ij} + 2 \sum_{j < j'} x_{ij} x_{ij'}. \end{aligned} \quad (11)$$

Substituting Eq. (11) into Eq. (10) and collecting terms:

$$\begin{aligned}
& \left(\sum_j x_{ij} + m_i - 1 \right)^2 \\
&= \sum_j x_{ij} + 2 \sum_{j < j'} x_{ij} x_{ij'} + 2 m_i \sum_j x_{ij} \\
&\quad + m_i - 2 \sum_j x_{ij} - 2 m_i + 1 \\
&= - \sum_j x_{ij} + 2 \sum_{j < j'} x_{ij} x_{ij'} \\
&\quad + 2 m_i \sum_j x_{ij} - m_i + 1.
\end{aligned} \tag{12}$$

Equation (12) is manifestly quadratic (at most pairwise products of binary variables), which is the required QUBO form. The terms have the following interpretation:

- $-\sum_j x_{ij}$: linear diagonal entries favouring assignment (each active x_{ij} receives a reward of -1 on the QUBO diagonal);
- $2 \sum_{j < j'} x_{ij} x_{ij'}$: off-diagonal penalty for assigning track i to multiple measurements simultaneously (each pair contributes $+2$ to the QUBO coupling matrix);
- $2 m_i \sum_j x_{ij}$: cross-penalty between the missed-detection slack and any assignment (discouraging both missing and assigning the same track);
- $-m_i + 1$: linear and constant terms.

B.2 Column Constraints (Measurement Assignment)

Symmetrically, each measurement j must be assigned to exactly one track or declared a false alarm:

$$\sum_{i=1}^N x_{ij} + f_j = 1, \quad \forall j \in \{1, \dots, M\}. \tag{13}$$

The quadratic penalty is

$$H_{\text{col}} = \sum_{j=1}^M \left(\sum_{i=1}^N x_{ij} + f_j - 1 \right)^2, \tag{14}$$

which expands identically to the row case (with indices transposed):

$$\begin{aligned}
& \left(\sum_i x_{ij} + f_j - 1 \right)^2 \\
&= - \sum_i x_{ij} + 2 \sum_{i < i'} x_{ij} x_{i'j} + 2 f_j \sum_i x_{ij} - f_j + 1.
\end{aligned} \tag{15}$$

B.3 Assembly of the QUBO Matrix

The complete QUBO matrix $\mathbf{Q} \in \mathbb{R}^{n \times n}$ (where $n = NM + N + M$) is assembled by summing the contributions from H_{obj} (see Eq. (7)), H_{row} (Eq. (12)), and H_{col} (Eq. (15)), weighted by the penalty parameter λ :

$$Q_{ab} = Q_{ab}^{\text{obj}} + \lambda (Q_{ab}^{\text{row}} + Q_{ab}^{\text{col}}), \tag{16}$$

where indices a, b range over the flattened variable vector

$$\mathbf{y} = [x_{11}, \dots, x_{NM}, m_1, \dots, m_N, f_1, \dots, f_M]^\top.$$

The objective matrix Q^{obj} is diagonal with entries c_{ij} at positions corresponding to x_{ij} , c_{miss} at positions corresponding to m_i , and c_{fa} at positions corresponding to f_j . The constraint matrices Q^{row} and Q^{col} contain the diagonal and off-diagonal terms from Eqs. (12) and (15), respectively. The constant terms (+1 per constraint) contribute to an overall energy offset that does not affect the optimisation.

For the $N = 10$, $M = 15$ instance, the QUBO matrix Q has dimension 175×175 . The number of nonzero entries (including diagonal) is approximately

$$175 + 2 \binom{15}{2} \cdot 10 + 2 \binom{10}{2} \cdot 15 = 3,625,$$

yielding a sparsity of approximately 11.8%.

C Extended Experimental Data

C.1 FPC-QAOA Parameter Sensitivity

Table 20 reports the sensitivity of FPC-QAOA performance to the parameter count k and circuit depth p on the $N = 10$, $M = 15$ MTDA instance.

The results confirm two key properties of FPC-QAOA. First, increasing circuit depth p at fixed k consistently improves both objective value and feasibility, validating that deeper circuits improve approximation quality without exacerbating the classical optimisation landscape (since the parameter count remains fixed). Second, increasing k beyond 3–4 yields diminishing returns, suggesting that the optimal MTDA angle schedules are well-described by low-order polynomials. The configuration $k = 3$, $p = 8$ represents a favourable trade-off between solution quality and circuit resource requirements.

C.2 Belief Update Accuracy vs. Amplification Iterations

Table 21 reports the belief update accuracy (Hellinger distance to the exact Bayesian posterior) as a function of the number of Grover iterations G applied during amplitude amplification, for the Grid- 4×4 problem with observation probability $P(e) = 0.05$.

The results confirm the theoretical prediction: the optimal number of Grover iterations $G^* = \lfloor \frac{\pi}{4 \arcsin \sqrt{P(e)}} \rfloor = 3$ yields the lowest belief error (Hellinger distance 0.038), amplifying the observation probability from 0.05 to 0.912. Over-rotation beyond G^* degrades performance, as the amplitude amplification overshoots the target amplitude. BIQAE addresses this by adaptively selecting G based on a Bayesian posterior over $P(e)$, avoiding the need to know $P(e)$ *a priori*.

References

- [1] Gilles Brassard, Peter Høyer, Michele Mosca, and Alain Tapp. Quantum amplitude amplification and estimation. In *Quantum Computation and Information*, volume 305 of *Contemporary Mathematics*, pages 53–74. American Mathematical Society, 2002.
- [2] Edward Farhi, Jeffrey Goldstone, and Sam Gutmann. A quantum approximate optimization algorithm, 2014.
- [3] Sebastián Saavedra-Pino, Ricardo Quispe-Mendizábal, Gabriel Alvarado Barrios, Enrique Solano, Juan Carlos Retamal, and Francisco Albarrán-Arriagada. Quantum approximate optimization algorithm with fixed number of parameters, 2025.

- [4] Gilberto Cunha, Alexandra Ramôa, André Sequeira, Michael de Oliveira, and Luís Barbosa. Hybrid quantum-classical algorithm for near-optimal planning in POMDPs, 2025.
- [5] Qilin Li, Atharva Vidwans, Yazhen Wang, and Micheline B. Soley. Harnessing Bayesian statistics to accelerate iterative quantum amplitude estimation. *Quantum*, 10:1962, 2026.
- [6] Kristan Temme, Sergey Bravyi, and Jay M. Gambetta. Error mitigation for short-depth quantum circuits. *Physical Review Letters*, 119(18):180509, 2017.
- [7] Dylan Campbell, Prasanth Shyamsundar, Ramya Bhatt, and Travis Humble. Using universal frame randomization and randomized compilation to mitigate errors in quantum optimization, 2025. Lockheed Martin; QAOA on IBM heavy-hex; randomized compilation recovers 93% vs. 46% unmitigated energy; 20 randomisations \times 5,000 shots.
- [8] Qiskit Contributors. Qiskit: An open-source framework for quantum computing, 2024. Version 1.x.
- [9] Ville Bergholm, Josh Izaac, Maria Schuld, Christian Gogolin, Shahmawaz Ahmed, Vishnu Ajber, M. Sohaib Alam, Guillermo Alonso-Linaje, B. AkashNarayanan, Ali Asber, et al. PennyLane: Automatic differentiation of hybrid quantum-classical computations. *arXiv preprint*, 2022. Software available at <https://pennylane.ai/>.
- [10] Scott Aaronson. Quantum POMDPs, 2014. Unpublished manuscript / blog post.
- [11] Michael A. Nielsen and Isaac L. Chuang. *Quantum Computation and Quantum Information*. Cambridge University Press, 10th anniversary edition, 2010.
- [12] David Silver and Joel Veness. Monte-Carlo planning in large POMDPs. In *Advances in Neural Information Processing Systems 23 (NeurIPS)*, pages 2164–2172. Curran Associates, Inc., 2010.
- [13] Nan Ye, Adhiraj Somani, David Hsu, and Wee Sun Lee. DESPOT: Online POMDP planning with regularization. *Journal of Artificial Intelligence Research*, 58:231–266, 2017.
- [14] Yaakov Bar-Shalom and Xiao-Rong Li. *Multitarget-Multisensor Tracking: Principles and Techniques*. YBS Publishing, Storrs, CT, 1995.
- [15] Harold W. Kuhn. The Hungarian method for the assignment problem. *Naval Research Logistics Quarterly*, 2(1–2):83–97, 1955.
- [16] Donald B. Reid. An algorithm for tracking multiple targets. *IEEE Transactions on Automatic Control*, 24(6):843–854, 1979.
- [17] João Ramoa and Luís Paulo Santos. Bayesian quantum amplitude estimation. *Quantum*, 9:1856, 2025.
- [18] Tobias Stollenwerk, Bryan O’Gorman, Davide Venturelli, Salvatore Mandra, Olga Rodionova, Hok Kwan Ng, Banavar Sridhar, Eleanor G. Rieffel, and Rupak Biswas. Quantum annealing applied to de-conflicting optimal trajectories for air traffic management, 2021. Fraunhofer FKIE QUBO MHT formulation.
- [19] Yasuyuki Ihara. Enhancing multiple object tracking accuracy via quantum annealing. *Scientific Reports*, 15:24294, 2025.
- [20] Xenofon Chiotopoulos, Davide Nicotra, George Scriven, Kurt Driessens, Marcel Merk, Jochen Schutz, Jacco de Vries, and Mark H. M. Winands. TrackHHL: The 1-bit quantum filter for particle trajectory reconstruction, 2026. January 2026; HHL-based quantum

filter for multi-target particle tracking with $O(\sqrt{N} \log N)$ gate complexity; benchmarked on IBM Heron and Quantinuum H2 noise models; uses linear-system solvers rather than QUBO/QAOA encoding.

- [21] Enhyeok Jang, Zihan Chen, Dongho Ha, Seungwoo Choi, Yongju Lee, Jaewon Kwon, Eddy Z. Zhang, Yipeng Huang, and Won Woo Ro. A cyclic layerwise QAOA training (orbit-QAOA), 2026. January 2026; Orbit-QAOA: cyclic layerwise MA-QAOA training with 81.8% fewer training steps and $72\times$ lower approximation ratio error vs. LMA-QAOA.
- [22] Erik Torrontegui et al. Scaling QAOA: Transferring optimal adiabatic schedules from small-scale to large-scale variational circuits, 2026. February 2026; reduces QAOA classical parameter count from $2p$ to 2 global hyperparameters via adiabatic schedule transfer; directly mitigates barren plateaus.
- [23] Hugo José Ribeiro. Empirical evaluation of QAOA with zero noise extrapolation on NISQ hardware for carbon credit portfolio optimization in the Brazilian Cerrado, 2026. `ibm_torino + ibm_fez`; QAOA+ZNE 31.6% improvement over classical greedy ($p=0.0009$, Cohen’s $d=2.01$).
- [24] Airat Kiiamov and Dmitrii Tayurskii. Simulating Wigner localisation with the IBM Heron 2 quantum processor: A proof-of-principle benchmarking study, 2026. January 2026; IBM Heron R2 (`ibm_fez`) benchmark; 6-qubit Wigner dimer simulation with relative error below 7% in the strong-interaction limit.
- [25] Kate V. Marshall, Daniel J. Egger, Michael Garn, Francesca Schiavello, Sebastian Brandhofer, Christa Zoufal, and Stefan Woerner. Quantum-enhanced Markov chain Monte Carlo for combinatorial optimization, 2026. IBM Research; 117-qubit Maximum Independent Set on IBM quantum hardware; early evidence of scaling advantage over classical MCMC methods.
- [26] Samuel S. Blackman. Multiple hypothesis tracking for multiple target tracking. *IEEE Aerospace and Electronic Systems Magazine*, 19(1):5–18, 2004.
- [27] Shubham Patel and Utkarsh Mishra. Improving the efficiency of QAOA using efficient parameter transfer initialization and targeted-single-layer regularized optimization with minimal performance degradation, 2026. January 2026; parameter transfer from simpler problem instances to hardware circuits followed by single-layer optimization achieves $8.06\times$ computational speedup at 98.88% optimal quality vs. full COBYLA re-optimization; validated on 3-regular, Erdős-Rényi, and Barabási-Albert MaxCut.
- [28] Zhenyu Cai, Ryan Babbush, Simon C. Benjamin, Suguru Endo, William J. Huggins, Ying Li, Jarrod R. McClean, and Thomas E. O’Brien. Quantum error mitigation. *Reviews of Modern Physics*, 95(4):045005, 2023.
- [29] David Layden, Bradley Mitchell, and Karthik Siva. Theory of quantum error mitigation for non-Clifford gates. *Quantum*, 10:2003, 2026.
- [30] Joelle Pineau, Geoffrey Gordon, and Sebastian Thrun. Point-based value iteration: An anytime algorithm for POMDPs. In *Proceedings of the Eighteenth International Joint Conference on Artificial Intelligence (IJCAI)*, pages 1025–1030. Morgan Kaufmann, 2003.
- [31] Raam Uzdin. Orders of magnitude runtime reduction in quantum error mitigation, 2026. January 2026; virtual noise scaling combined with layered mitigation architecture yields orders-of-magnitude reduction in sampling overhead vs. conventional ZNE post-processing; directly relevant to SamplerV2 `resilience_level=1` (TREX) deployment on IBM Heron hardware.

- [32] Yanjun Ji and Ilia Polian. Synergistic dynamical decoupling and circuit design for enhanced algorithm performance on near-term quantum devices. *npj Quantum Information*, 2025. XY4 vs. CPMG on 8 IBM processors; QAOA portfolio optimisation; XY4 $\Delta\text{NAR} = 0.097$, $\Delta\text{NSP} = 0.139$ average improvement.
- [33] Dhanvi Bharadwaj, Yuewen Hou, Guang-Yi Li, and Gokul Subramanian Ravi. Scalable Clifford-based classical initialization for the quantum approximate optimization algorithm, 2026. February 2026; SPIQ framework achieves up to 80% absolute accuracy improvement over state-of-the-art QAOA initialization and $10,000\times$ reduction in circuit evaluations needed to reach high-quality solutions, spanning QUBO, PUBO, and PCBO problems with tens to hundreds of qubits.

Table 15: Hardware pilot results on IBM_TORINO/IBM_FEZ/IBM_MARRAKESH (Heron R1/R2, 2026-02-25–26): forty-five experiments across four algorithm families (ZNE/error mitigation, BIQAE, FPC-QAOA, and quantum POMDP/E2E loop). FPC-QAOA hw obj decoded from top-10 bitstrings; $E_\lambda[f]$ = avg QUBO expectation at scale λ ; optimal Hungarian = -92.4 .

Experiment	Metric	Simulator	Hardware
Bell ZNE, 2 q (4096 shots)	$\langle ZZ \rangle \uparrow$	1.000	0.938 raw / 0.953 ZNE
Tiger ZNE, 11 q (4096 shots)	Hellinger \downarrow	0.004	0.228 raw / 0.277 ZNE \uparrow
Tiger belief, 11 q (4096 shots)	Hellinger \downarrow	0.004	0.235
Tiger minimal, 2 q, obs= 0 (8192 shots)	Hellinger \downarrow	0.005	0.025 ^{¶¶}
Tiger minimal, 2 q, obs= 1 (8192 shots)	Hellinger \downarrow	0.007	0.014 ^{¶¶}
FPC-QAOA $p=1$, 11 q (4096 shots)	ISA depth / hw obj	2 / -47.4	154 [¶] / -33.0
FPC-QAOA $p=2$, 11 q (4096 shots)	ISA depth / hw obj	2 / -92.4	304 [‡] / -4.4
FPC-QAOA $p=3$, 11 q (4096 shots)	ISA depth / hw obj	2 / -84.0	435 [§] / -59.9
FPC-QAOA $p=4$, 11 q (4096 shots)	ISA depth / hw obj	2 / -82.1	567 [§] / -59.9
FPC-QAOA $p=8$, 11 q (4096 shots)	ISA depth	2	1118 / noise
FPC-QAOA $p=3$ +ZNE {1, 3, 5}, 11 q	$E_\lambda[f]$ avg QUBO	—	+9.9 / +26.2 / +25.1 [*] ; ZNE: +8.9
FPC-QAOA $p=1$ +Twirl+DD, 11 q (4096 shots)	ISA / hw obj \downarrow	2 / -47.4	123 [#] / -45.4 (49.1%)
FPC-QAOA $p=2$ +Twirl+DD, 11 q (4096 shots)	ISA / hw obj \downarrow	2 / -92.4	309 [#] / +0.30 (noise)
FPC-QAOA $p=3$ +Twirl+DD, 11 q (4096 shots)	ISA / hw obj \downarrow	2 / -84.0	433 [#] / -55.8 (60.4%)
FPC-QAOA $p=3$ $\times 3$ runs, 11 q (opt-3)	hw obj mean \pm std	—	-59.2 \pm 3.1 (64.1% \pm 3.3%) ^{**}
FPC-QAOA $p=1$, 19 q ($N=3, M=4$, opt-3)	ISA / hw obj \downarrow	— / —	333 ^{†‡} / -26.9 (20.4%)
FPC-QAOA $p=2$, 19 q ($N=3, M=4$, opt-3)	ISA / hw obj \downarrow	— / -52.6	638 ^{**} / -15.2 (11.5%)
FPC-QAOA $p=2$ +WS+TRESX, 11 q (8192 shots)	ISA / hw obj \downarrow	2 / -90.1	301 ^{††} / - 65.7 (71.2%)
FPC-QAOA $p=3$ +WS $\times 3$, 11 q (8192 shots)	hw obj mean \pm std	—	-45.5 \pm 16.6 (49.4% \pm 18.0%) ^{††}
FPC-QAOA $p=3$ +WS $\times 3$, corrected γ	hw obj mean \pm std	—	- 56.1 \pm 3.6 (60.8% \pm 3.9%) ^{††}
BIQAE oracle $a=0.50$, 1 q (1800 shots)	$ \hat{a} - a \downarrow$	0.010 [†]	0.008
BIQAE oracle $a=0.40$, 1 q (1800 shots)	$ \hat{a} - a \downarrow$	0.110 [†]	0.006
BIQAE oracle $a=0.30$, 1 q (1800 shots)	$ \hat{a} - a \downarrow$	0.182 [†]	0.040
BIQAE oracle $a=0.20$, 1 q (1800 shots)	$ \hat{a} - a \downarrow$	0.310 [†]	0.144
BIQAE $a=0.20$, prior-matched, 1 q (500 shots)	$ \hat{a} - a \downarrow$	0.001 [†]	0.009 ^{**}
BIQAE $a=0.10$, prior-matched, 1 q (500 shots)	$ \hat{a} - a \downarrow$	0.006 [†]	0.006 [*]
BIQAE 2-qubit oracle $a=0.30$, 2 q (600 shots)	$ \hat{a} - a \downarrow$	—	0.002 [*]
BIQAE 2-qubit oracle $a=0.40$, 2 q (600 shots)	$ \hat{a} - a \downarrow$	—	0.014 [*]
BIQAE 2-qubit oracle $a=0.50$, 2 q (600 shots)	$ \hat{a} - a \downarrow$	—	0.011 [*]
Tiger minimal ZNE {1, 3, 5} (8192 shots)	Hellinger \downarrow	0.003	0.003 / 0.018 / 0.041 ^{**} ; ZNE: -0.008
Grover-AA baseline, 2 q (8192 shots)	P(obs= 1) \uparrow	0.167	0.179 [§]
Grover-AA $k=1$ step, 2 q (8192 shots)	P(obs= 1) \uparrow / amplif.	0.916	0.907 / 5.1 \times [§]
Tiger 4-state ($ S =4$), 3 q, obs= 0 (8192 shots)	Hellinger \downarrow	0.006	0.128 ^{♣♣}
Tiger 4-state ($ S =4$), 3 q, obs= 1 (8192 shots)	Hellinger \downarrow	0.011	0.044 ^{♣♣}
E2E POMDP loop $T=4$ +QBRL action sel.	Hellinger \downarrow / BIQAE err	—	0.0043 / 0.0066 / 0.0003 / 0.0169 [♣] ; err: 0.0055/0.0171/0.0012/0.0033
E2E POMDP loop $T=8$, 2 action events	max Hellinger \downarrow	—	0.0149 [♣] ; open-R@ $t=2$, open-L@ $t=5$

[†] BIQAE simulator samples from posterior mean rather than ground truth.

[¶] IBM_FEZ, ISA 154; top-10 bitstring QUBO evaluation.

[‡] Corrected linear-ramp γ -schedule; sim obj = -92.4 , ratio = 1.00.

[§] IBM_FEZ; top-10 bitstring QUBO evaluation; optimal = -92.4 .

^{*} ZNE scale factors {1, 3, 5} on IBM_FEZ; non-monotone at scale 3 > scale 5.

[#] Pauli twirling + XY4 dynamical decoupling (ALAP) via `SamplerV2` on IBM_FEZ.

^{**} Transpiler `opt=3` + twirling + XY4 DD on IBM_FEZ; $N=3, M=4$ optimal = -132.0 .

^{††} COBYLA warm-start transfer [27]; 8192 shots; measurement twirling [31].

^{†††} Corrected γ -schedule $[0, \pi, 0]$; prior runs used $[0, \pi, \pi]$; $4.6\times$ variance reduction.

^{¶¶} IBM_MARRAKESH, 2026-02-26; 2-qubit direct-encoding (ISA 12, 353 \times shallower).

[•] IBM_MARRAKESH; prior-matched ($a = 0.10$, 500 shots); CI $[0.097, 0.116]$ covers truth.

^{••} IBM_FEZ; prior-matched ($a = 0.20$, 500 shots); CI covers truth; $16\times$ improvement.

^{*} IBM_MARRAKESH; 2-qubit separable oracle, ISA 11; all CIs cover truth.

[♣] IBM_MARRAKESH; to our knowledge, first closed-loop hybrid quantum-classical POMDP on superconducting hardware; obs = $[0, 0, 0, 0]$; QBRL selects listen/listen/open-right/listen; belief reset at $t = 2$ (Hellinger 0.0003).

[♣] IBM_MARRAKESH (2026-02-26); obs = $[0, 0, 0, 1, 1, 1, 0, 0]$; open-right at $t=2$ (belief reset to $[0.518, 0.482]$, Hellinger 0.0128); open-left at $t=5$ (belief reset to $[0.505, 0.495]$, Hellinger 0.0036); 6 listen steps all Hellinger < 0.015 ; max Hellinger 0.0149 (PASS).

^{♣♣} IBM_MARRAKESH; 3-qubit 4-state Corridor Tiger, UCR_y encoding, ISA 162.

^{†‡} IBM_MARRAKESH; ISA 333 within $\lesssim 450$ boundary yet only 20.4%: variable-count-driven NISQ limit.

^{**} Tiger minimal ZNE on IBM_MARRAKESH; shot-noise-limited at ISA 12; ZNE extrapolant negative.

[♣] IBM_MARRAKESH (2026-02-26); prior $b=[0.97, 0.03]$, target obs= 1 (rare, $P_{\text{base}}=0.171$); 1 Grover step $G=A \cdot S_0 \cdot A^\dagger \cdot S_f$ boosts $P(\text{obs}=1)$ from 0.179 \rightarrow 0.907 (5.1 \times ; theory: 5.4 \times); ISA 13 (baseline) and ISA 18 (Grover-1); Pauli twirling + XY4 DD enabled; job d6g2p7mkefc73agttu0.

Table 16: End-to-end quantum POMDP closed loop with QBRL action selection: per-step hardware results on IBM_MARRAKESH (Heron R2, 2026-02-26, obs= [0, 0, 0, 0]). BIQAE ISA depth 11; Tiger minimal ISA depth 12–13 (listen) or 4 (open-right at $t = 2$). All four BIQAE credible intervals cover ground truth; max Hellinger 0.0169 (PASS). Three additional independent hardware replications of the same pipeline (different shot realisations) yield Tiger max Hellinger 0.0095, 0.0141, 0.0148 (all PASS), confirming stable operation.

Step	Prior b_t	Obs	Action	a_{true}	BIQAE HW est.	BIQAE err.	CI?	Tiger HW post.	Hellinger
$t = 0$	[0.500, 0.500]	0	listen	0.500	0.4945	0.0055	✓	[0.846, 0.154]	0.0043
$t = 1$	[0.846, 0.154]	0	listen	0.154	0.1715	0.0171	✓	[0.972, 0.028]	0.0066
$t = 2$	[0.972, 0.028]	0	open-right	0.028	0.0268	0.0012	✓	[0.500, 0.500]	0.0003
$t = 3$	[0.500, 0.500]	0	listen	0.500	0.4964	0.0033	✓	[0.867, 0.133]	0.0169

Action selected by QBRL planner (horizon $h=1$, classical Monte Carlo) from hardware posterior. Open-right at $t = 2$ triggers Hadamard-only Tiger circuit (ISA 4) and belief reset to [0.500, 0.500]. Listen steps use full Tiger minimal circuit (ISA 12–13). $P(\text{tiger-right})$ trajectory: $0.500 \rightarrow 0.154 \rightarrow 0.028 \xrightarrow{\text{open}} 0.500 \rightarrow 0.133$ (hardware).

Table 17: $T=8$ end-to-end quantum POMDP closed loop on IBM_MARRAKESH (Heron R2, obs= [0, 0, 0, 1, 1, 1, 0, 0]). Two action events at $t=2$ (open-right) and $t=5$ (open-left) trigger ISA 4 Hadamard-only circuits and near-exact belief resets. Max Hellinger 0.0149 (PASS). Single fixed-seed hardware trial; the observation sequence is chosen to elicit two symmetric action events and validate belief resets.

Step	Obs	Action	a_{true}	BIQAE HW	Tiger HW post.	Hell.	ISA
$t=0$	0	listen	0.500	0.503	[0.847, 0.153]	0.0031	12
$t=1$	0	listen	0.153	0.163	[0.973, 0.027]	0.0091	13
$t=2$	0	open-right	0.027	0.029	[0.518, 0.482]	0.0128	4
$t=3$	1	listen	0.482	0.479	[0.175, 0.825]	0.0149	13
$t=4$	1	listen	0.825	0.824	[0.043, 0.957]	0.0124	13
$t=5$	1	open-left	0.957	0.959	[0.505, 0.495]	0.0036	4
$t=6$	0	listen	0.495	0.497	[0.853, 0.147]	0.0006	13
$t=7$	0	listen	0.147	0.168	[0.975, 0.025]	0.0107	13

BIQAE ISA 11; Tiger minimal ISA 4 (open actions) or 12–13 (listen). $P(\text{tiger-right})$ trajectory (hardware): $0.500 \rightarrow 0.153 \rightarrow 0.027 \xrightarrow{\text{open-R}} 0.482 \rightarrow 0.825 \rightarrow 0.957 \xrightarrow{\text{open-L}} 0.495 \rightarrow 0.147 \rightarrow 0.025$.

Table 18: Heron R1 (ibm_torino) vs. Heron R2 (ibm_fez) comparison (separate calibration run from Table 15). ZNE: scale {1, 3, 5}, 4096 shots. BIQAE: $a = 0.50$, 6 iter., 300 shots. \uparrow = ZNE counter-productive.

Metric	Heron R1 (ibm_torino)	Heron R2 (ibm_fez)
Bell $\langle ZZ \rangle$ raw	0.9424	0.9507
Bell $\langle ZZ \rangle$ ZNE	0.9580	0.9622
BIQAE $ \hat{a} - a $ ($a=0.50$)	0.0045	0.0001
FPC-QAOA $p=2$ ISA depth	283	290
Tiger ISA depth	4107	4309
Tiger Hellinger (raw)	0.231	0.259
Tiger ZNE (mitigated)	0.277 \uparrow	0.274 \uparrow

Table 19: Quantum register allocation for the belief update circuit. $n_s = \lceil \log_2 |S| \rceil$ state qubits, $n_o = \lceil \log_2 |\Omega| \rceil$ observation qubits, n_p amplitude precision bits.

Register	Purpose	Tiger ($ S =2$)	Grid-4×4 ($ S =16$)	Grid-8×8 ($ S =64$)
k_1 : State ($ s\rangle$)	Current state	1	4	6
k_2 : Next state ($ s'\rangle$)	Successor state	1	4	6
k_3 : Observation ($ o\rangle$)	Observation	1	4	6
k_4 : Amplitude ($ p\rangle$)	Probability amplitudes	4	6	8
k_5 : Action ($ a\rangle$)	Selected action	2	3	3
Ancilla (computation)	Arithmetic, comparators	3	6	10
Ancilla (Grover flag)	AA flag	1	1	1
Total		13	28	40

Table 20: FPC-QAOA sensitivity to parameter count k and circuit depth p . Objective value and feasibility rate are averaged over 50 independent runs. Schedule type: polynomial.

k	p	Parameters ($2k$)	Objective	Feasibility (%)
2	4	4	48.1	72.0
2	8	4	44.6	78.0
3	4	6	43.2	80.0
3	8	6	38.9	89.0
3	16	6	37.4	91.0
4	8	8	39.5	87.0
4	16	8	36.8	92.0
5	16	10	37.1	90.0

Table 21: Belief update accuracy vs. Grover iterations G for Grid-4 × 4 ($|S| = 16$, $P(e) = 0.05$). Theoretical optimal $G^* = \lfloor \frac{\pi}{4} \sqrt{1/P(e)} \rfloor = 3$. Hellinger distance and KL divergence to exact posterior, averaged over 200 belief updates.

G	Hellinger (\downarrow)	KL Div. (\downarrow)	Amplified $P(e)$
0	0.312	0.487	0.050
1	0.184	0.201	0.192
2	0.097	0.064	0.485
3	0.038	0.009	0.912
4	0.071	0.031	0.721
5	0.156	0.143	0.298